Springer

Dear Author:

Please find attached the final pdf file of your contribution, which can be viewed using the Acrobat Reader, version 3.0 or higher. We would kindly like to draw your attention to the fact that copyright law is also valid for electronic products. This means especially that:

- You may print the file and distribute it amongst your colleagues in the scientific community for scientific and/or personal use.

- You may make your article published by Springer-Verlag available on your personal home page provided the source of the published article is cited and Springer-Verlag and/or other owner is mentioned as copyright holder. You are requested to create a link to the published article in Springer's internet service. The link must be accompanied by the following text: "The original publication is available at springerlink.com". Please use the appropriate DOI for the article. Articles disseminated via SpringerLink are indexed, abstracted and referenced by many abstracting and information services, bibliographic networks, subscription agencies, library networks and consortia.

- Without having asked Springer-Verlag for a separate permission your institute/your company is not allowed to place this file on its homepage.

- You may not alter the pdf file, as changes to the published contribution are prohibited by copyright law.

- Please address any queries to the production editor of the journal in question, giving your name, the journal title, volume and first page number.

Yours sincerely,

Springer-Verlag

Climate Dynamics (2003) 21: 423–446
DOI 10.1007/s00382-003-0337-1

**D. E. Waliser · K. Jin · I.-S. Kang · W. F. Stern
S. D. Schubert · M. L. C. Wu · K.-M. Lau · M.-I. Lee
V. Krishnamurthy · A. Kitoh · G. A. Meehl · V. Y. Galin
V. Satyan · S. K. Mandke · G. Wu · Y. Liu · C.-K. Park**

AGCM simulations of intraseasonal variability associated with the Asian summer monsoon

Received: 8 August 2002 / Accepted: 7 April 2003 / Published online: 30 August 2003
© Springer-Verlag 2003

Abstract The intraseasonal variability associated with the Asian summer monsoon as simulated by a number of atmospheric general circulation models (AGCMs) are analyzed and assessed against observations. The model data comes from the Monsoon GCM Intercomparison project initiated by the CLIVAR/Asian–Australian Monsoon Panel. Ten GCM groups, i.e., the Center for Ocean–Land–Atmosphere Studies (COLA), Institute of Numerical Mathematics (DNM), Goddard Space Flight Center (GSFC), Geophysical Fluid Dynamics Laboratory (GFDL), Institute of Atmospheric Physics (IAP), Indian Institute of Tropical Meteorology (IITM), Meteorological Research Institute (MRI), National Center for Atmospheric Research (NCAR), Seoul National University (SNU), and the State University of New York (SUNY), participated in the intraseasonal component of the project. Each performed a set of 10 ensemble simulations for 1 September 1996–31 August 1998 using the same observed weekly SST values but with different initial conditions. The focus is on the spatial and seasonal variations associated with intraseasonal variability (ISV) of rainfall, the structure of each model's principal mode of spatial-temporal variation of rainfall [i.e. their depiction of the Intraseasonal Oscillation (ISO)], the teleconnection patterns associated with each model's ISO, and the implications of the models' ISV on seasonal monsoon predictability. The results show that several of the models exhibit ISV levels at or above that found in observations with spatial patterns of ISV that resemble the observed pattern. This includes a number of rather detailed features, including the relative distribution of variability between ocean and land regions. In terms of the area-averaged variance, it is found that the fidelity of a model to represent NH summer versus winter ISV appears to be strongly linked. In addition, most models' ISO patterns do exhibit some form of northeastward propagation. However, the model ISO patterns are typically less coherent, lack sufficient eastward propagation, and have smaller zonal and meridional spatial scales than the observed patterns, and are often limited to one side or the other of the maritime continent. The most pervasive and problematic feature of the models' depiction of ISV and/or their ISO patterns is the overall lack of variability in the equatorial Indian Ocean. In some cases, this characteristic appears

D. E. Waliser (✉)
Marine Sciences Research Center, State University of New York, Stony Brook, NY 11794-5000, USA
E-mail: duane.waliser@sunysb.edu

K. Jin · I.-S. Kang · M.-I. Lee
School of Earth and Environmental Sciences, Seoul National University, Seoul, Korea

W. F. Stern
Geophysical Fluid Dynamics Laboratory, Princeton University, Princeton, NJ, USA

S. D. Schubert · M. L. C. Wu
Data Assimilation Office, NASA/GSFC, Greenbelt, MD, USA

K.-M. Lau
Climate and Radiation Branch, NASA/GSFC, Greenbelt, MD, USA

V. Krishnamurthy
Center for Ocean–Land–Atmosphere Studies, Calverton, MD, USA

A. Kitoh
Meteorological Research Institute, Tsukuba, Ibaraki, Japan

G. A. Meehl
National Center for Atmospheric Research, Boulder, CO, USA

V. Y. Galin
Institute of Numerical Mathematics of Russian Academy of Sciences, Moscow, Russia

V. Satyan · S. K. Mandke
Indian Institute of Tropical Meteorology, Pune, India

G. Wu · Y. Liu
LASG, Institute of Atmospheric Physics, Beijing, People's Republic of China

C.-K. Park
Climate Prediction Division, Korea Meteorological Administration, Seoul, Korea

to result from some models forming double convergence zones about the equator rather than one region of strong convergence on the equator. This shortcoming results in a poor representation of the local rainfall pattern and also significantly influences the models' representations of the global-scale teleconnection patterns associated with the ISO. Finally, analysis of the model ensemble shows a positive relationship between the strength of a model's ISV of rainfall and its intra-ensemble variability of seasonal monsoon rainfall. The implications of this latter relation are discussed in the context of seasonal monsoon predictability.

1 Introduction

The tropical intraseasonal oscillation (ISO) plays an extremely influential role in the nature and evolution of the Asian summer monsoon. In particular, it has a dominant influence over monsoon onset and break activity (e.g., Yasunari 1979; Lau and Chan 1986; Lau et al. 1988; Kang et al. 1989; Nakazawa 1992; Wang and Xu 1997; Wu and Zhang 1998; Kang et al. 1999; Kemball-Cook and Wang 2001; Liu et al. 2002). In fact, the variance associated with intraseasonal monsoon fluctuations typically exceeds the variance associated with interannual fluctuations in almost all Eastern Hemisphere monsoon regions (e.g., Lau and Chan 1988; Waliser et al. 1993). As an illustration of these features, Fig. 1 compares total pentad anomaly (gray), intraseasonal (30–90 day), and interannual (>90 day) fluctuations in area-averaged rainfall over India and Southeast Asia for the 1994, 1995 and 1996 monsoons. From this figure, it is apparent that the intraseasonal time scale is a recurrent form of variability within the monsoon. Further, when this time scale is active, it comprises a significant fraction of the total anomalous variability, and as mentioned it is the main factor for determining the onsets and break periods of the monsoon.

Along with this strong influence on the monsoon itself, intraseasonal (and sub-monthly) convective activity in the Asian monsoon sector has also been linked to Northern Hemisphere (NH) summer time precipitation variability over the United States, Mexico and South America as well as to wintertime circulation anomalies over the Pacific–South American Sector (e.g., Nogues-Paegle and Mo 1997; Mo and Higgins 1998; Jones and Schemm 2000; Mo 2000b; Paegle et al. 2000). In addition, studies have also shown that particular phases of ISO convective anomalies are more favorable than others in regards to the development of tropical storms/hurricanes in both the Atlantic and Pacific sectors (e.g., Maloney and Hartmann 2000; Mo 2000a; Higgins and Shi 2001). While a wealth of effort has been directed towards developing and improving general circulation models (GCMs), this effort has not been driven to a great extent by obtaining a proper simulation of the monsoon or its associated variability (e.g., ISO). Even so, there has been considerable interest in model simulations and predictions of monsoon variations (e.g., Fennessy et al. 1994; Liang et al. 1995; Sperber and Palmer 1996; Lal et al. 1997; Soman and Slingo 1997; Goswami 1998; Webster et al. 1998; Martin 1999; Zachary and Randall 1999; Sperber et al. 2000; Kang et al. 2002a, b), most of this effort has been focused on monthly or longer time scales with considerably less consideration of sub-seasonal time scales. Unfortunately, even with these tremendous efforts there are still significant shortcomings in representing the basic annual

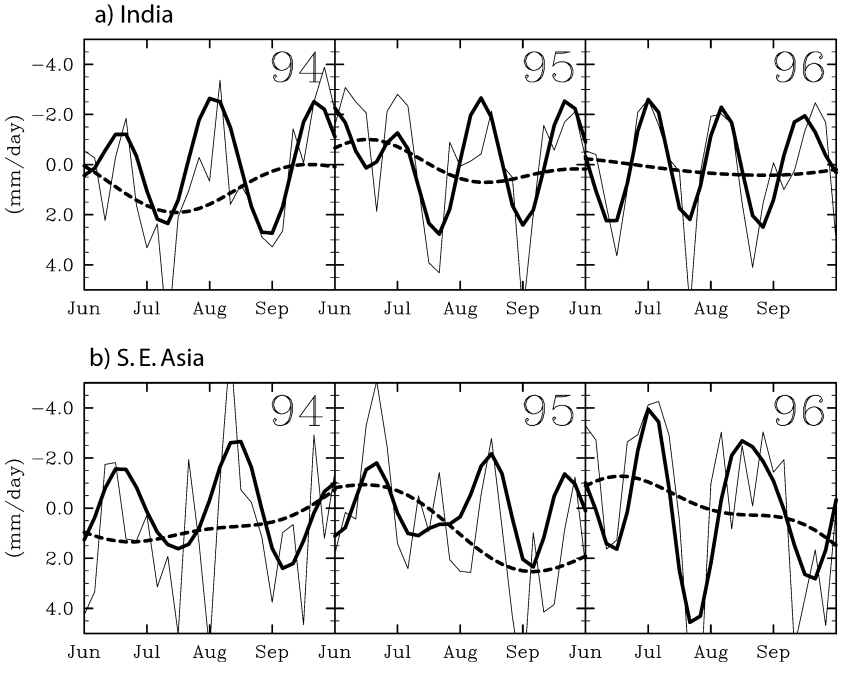

Fig. 1 June through September anomalous rainfall data for the years 1994, 1995 and 1996 for India (**a**) and Southeast Asia (**b**). The rainfall data are pentad values from Xie and Arkin (1997). The *thin gray lines* are pentad anomaly values, the *thick black lines* are 30–90 day bandpassed values, and the *dotted lines* are 90 day lowpass values. The data plotted for India are the domain-averages of the data grid points lying within India. The data plotted for Southeast Asia are the domain-averages of the data grid points encompassing the majority of Thailand, Laos, Cambodia, Vietnam and Indonesia

cycle associated with the summer monsoon, let alone its interannual anomalies.

Considering the extremely significant role that the intraseasonal time scale plays in the summer monsoon, along with the significant problems we are still having at simulating and predicting low-frequency monsoon variability, suggests that an examination is warranted of the character and quality of the intraseasonal variations simulated by atmospheric GCMs (AGCMs). Two aspects motivate such an examination. The first is that part of the shortcomings in GCM representations of low-frequency monsoon variations may be associated with this representations in the higher frequency components, such as the intraseasonal time scale. Thus an assessment of these shortcomings is needed to develop remedies which may in turn improve the seasonal and interannual time scale of monsoon simulations. The second is that apart from any potential for seasonal monsoon prediction, there is a tremendous need for providing and/or improving predictions of monsoon onset and break periods (Krishnamurti et al. 1992; Webster et al. 1998; Ramesh and Iyengar 1999; Waliser et al. 1999b, 2003). This will only come about via improved representation of the intraseasonal component of the monsoon in GCMs.

To date, there have only been a few efforts that help to characterize and assess GCM capabilities regarding intraseasonal variability of the Asian summer monsoon. The first is the Atmospheric Model Intercomparison Project (AMIP) study by Slingo et al. (1996) that examined the intraseasonal variability in 15 AGCMs. However, the focus of this study was on NH winter form of intraseasonal variability, namely the Madden-Julian Oscillation (MJO' Madden and Julian 1994), which involves the propagation of convective anomalies eastward along equator from the central Indian Ocean to the central Pacific Ocean/South Pacific Convergence Zone (SPCZ). Even so, the general conclusions of that study are likely to have bearing on the NH summer form of intraseasonal variability which involves the northeastward propagation of convective anomalies from the central Indian Ocean, over Southeast Asia, and into the northwest tropical Pacific Ocean (e.g., Wang and Rui 1990; Ferranti et al. 1997; Sperber et al. 2000). Those conclusions were that most AGCMs have difficulty in properly simulating the MJO in terms of strength, propagation speed, seasonality and interannual variability. The results of their analysis also suggested that models that simulate realistic basic states, including the annual cycle and basic relationships between warm sea surface temperatures (SSTs) and precipitation rate, tend to have better MJO simulations.

A second effort that examined intraseasonal variability in AGCMs was a recent study by Sperber et al. (2001). While the focus of that study was primarily on dynamical seasonal prediction of the Asian summer monsoon, the analysis included an assessment of how well the models reproduce subseasonal modes of variability. Their results showed that for many models, the dominant dynamical pattern of subseasonal variability is often simulated. Beyond this however, the AGCMs had difficulty in representing the pattern of precipitation associated with the dominant mode as well as difficulty in simulating most aspects of the higher order modes of subseasonal variability. In addition, that study found that the models usually fail to project the subseasonal modes onto the seasonal mean anomalies, even in cases where the mode may be influenced by surface boundary conditions.

Recently, Kang et al. (2002b) examined how well AGCMs simulate the climatological intraseasonal variation of the Asian summer monsoon. Their study showed that the simulated northward propagation of the climatological intraseasonal oscillations of precipitation occur 20–30 days earlier than the observations over the east Asian monsoon region. This result is in partial agreement with the case study of Wu et al. (2002) that indicated that the simulated and observed (individual) oscillations are approximately in quadrature, with the simulated responses leading by 5–10 days when referenced to the intraseasonal variability residing in the SST field. They suggested that this lead results from a suppression of the SST feedback that appears to be important to the simulation of tropical intraseasonal variability (Flatau et al. 1997; Sperber et al. 1997; Waliser et al. 1999a; Kemball-Cook et al. 2002).

Based on the need for a more direct assessment of the intraseasonal variability of Asian summer monsoon within state-of-the-art GCMs, this study examines the representation and realism of the NH summertime ISO variability that is exhibited within 10 AGCMs. The models examined in this study and the associated experimental framework are based on the Asian–Australian monsoon GCM intercomparison project, initiated by the International CLIVAR Asian–Australian Monsoon Panel. This intercomparison project involves examining a number of aspects associated with the monsoon, including the simulation character of the ENSO/Monsoon anomalies associated with the 1997–98 El Niño (Kang et al. 2002a), the climatological variations of the Asian summer monsoon (Kang et al. 2002b), the Asian–Australian monsoon variability during 1997–98 El Niño (Wang et al. 2003), and the SST-forced versus free character of the intraseasonal variability of the monsoon (Wu et al. 2002).

Since intraseasonal events are typically stochastic in nature and, to first order, tend not to be forced by the surface boundary conditions (Hendon et al. 1999; Slingo et al. 1999; Waliser et al. 2001; Wu et al. 2001), we do not focus on the simulation of specific events, nor do we try to emphasize the results of individual models. Rather, we focus on the performance of the models as a whole and seek to summarize the systematic errors that are common to the current AGCMs in simulating the intraseasonal variation of Asian summer monsoon and its connections with other components of the climate system.

The next section describes the experimental framework of the CLIVAR/GCM Monsoon Intercomparison Project, the model output obtained from that experiment as well as the observed data utilized in the present study. Section 3 presents the results of the comparison in terms of ISO strength and canonical space-time structure, downstream and extra-tropical teleconnection patterns, and the implications of the models' ISO variability on monsoon predictability. Section 4 closes with a brief summary of the results as well as some concluding remarks.

2 Experimental framework and data sources

The analysis is based on 10-member ensembles of two-year simulations from 10 different AGCMs made available through the CLIVAR/GCM Monsoon Intercomparison project. The AGCM simulations used here are from the Center for Ocean-Land-Atmosphere Studies (COLA; USA), Institute of Numerical Mathematics (DNM; Russia), Goddard Space Flight Center (GSFC; USA), Geophysical Fluid Dynamics Laboratory (GFDL; USA), Institute of Atmospheric Physics (IAP; China), Indian Institute of Tropical Meteorology (IITM; India), Meteorological Research Institute (MRI; Japan), National Center for Atmospheric Research (NCAR; USA), Seoul National University (SNU; Korea), and the State University of New York (SUNY/NASA-GLA; USA). A brief description of the participating models is given in Table 1. Further details of the model intercomparison project and the participating models can be found in Kang et al. (2002a). It is probably worth mentioning that four of the models (NCAR, GLA, GSFC, MRI) were included in the AMIP study of MJO variability during NH winter (Slingo et al. 1996), however all but the GLA AGCM have been modified since the time data was submitted for AMIP. In addition, only the DNM AGCM is common to the ten models listed above and the seven models examined by Sperber et al. (2001).

The 10-member ensemble AGCM simulations were performed for the period 1 September 1996 through 31 August 1998. Note that in terms of ENSO, the winter of 1996/97 and the summer of 1998 exhibited cool to near-neutral conditions, while the summer of 1997 and winter of 1997/98 were very warm phases (e.g., Bell et al. 1999; McPhaden 1999). The 10 ensemble members differ only in the initial atmospheric conditions. The SSTs are prescribed from the weekly SST data of Reynolds and Smith (1994). In addition to the ensembles, the models were run for the period 1979–98 with prescribed observed monthly SSTs. These longer runs were used to produce, for each model, a 5-day average (pentad) climatology that serves as a reference for analyzing the 1996–98 time period. The only exception is the GEOS model climatology that is for the shorter period of 1980–1992. The only variables saved with daily values were winds at 850 and 200 hPa, and precipitation. For this study, the variables used for examining ISV are pentad values of precipitation and 200 hPa velocity potential (hereafter, VP200). Validation data for rainfall and VP200 are obtained from the Xie and Arkin (1997) pentad rainfall estimates and the NCEP/NCAR renalaysis (Kalnay et al. 1996), respectively.

All AGCM and validation data were interpolated to a common spatial resolution of 2.5° latitude × 2.5° longitude. For the models, the VP200 fields were computed from the winds at the common resolution. To isolate the intraseasonal time scale the first two annual harmonics were removed and then a 30-point/pentad 20–90 day bandpass filter was applied. Hereafter, these intraseasonally bandpassed data will simply be referred to as filtered data. The edge effects of this filter resulted in the removal of the first and last 15 pentads of data from the data set, leaving a data record from 12 November 1996 to 14 June 1998. Most relevant to the present study is the removal of the 15 pentads from the end of the record, those that occur in the second of two summers of the simulation. Since in

Table 1 Description of the atmospheric GCMs participating in the CLIVAR/Asian–Australian Monsoon GCM intercomparison project

Group	Institution	Model	Resolution	Radiation	Convection	Land surface process	Cloud formulation
COLA	Center for Ocean–Land–Atmosphere Studies (USA)	COLA 1.11	R40L18	Lacis and Hansen (1974), Harshvardhan et al. (1987)	Relaxed Arakawa-Schubert (Moorthi and Suarez 1992)	Sib model, Xue et al. (1991)	Hou (1990) based on Slingo (1987)
DNM	Institute of Numerical Mathematics (Russia)	A5421	4°_5°, L21	Slingo (1989), Chou et al. (1993)	Betts (1986)	Volodin and Lykossov (1998)	Slingo (1987)
GEOS	NASA/GSFC (USA)	GEOS-2	2°_2.5°, L43	Chou and Suarez (1994)	RAS (Moorthi and Suarez 1992)	Schemm et al. (1992)	Slingo and Ritter (1985)
GFDL	Geophysical Fluid Dynamics Laboratory (USA)	DERF GFDLSM V197	T42L18	Lacis and Hansen (1974), Schwarzkopf and Fels (1991)	RAS (Moorthi and Suarez 1992)	Deardorff (1978)	Slingo (1987), Gordon (1992)
IAP	Institute of Atmosphereic Physics (China)	SAGCM 1.1	R15L9	ESFT shi (1981)	MCA (Manabe et al. 1965), No shallow convection	Sib model, Xue et al. (1991)	Prescribed
ITTM	Indian Institute of Tropical Meteorology (India)	HadAM2b V4.0, UKMO	2.5°_3.75°, L19	Ingram (1996), Slingo and Wilderspin (1985)	Mass flux penetrative convection scheme (Gregory and Rowntree 1990)	Smith (1990a)	Smith (1990b)
MRI	Meteorological Research Institute (Japan)	MRI GCM2	4°_5°, L15	Lacis and Hansen (1974), Shibata and Aokl (1989)	Arakawa-Schubert, Tokioka et al. (1988)	Katayama (1978), Kitoh et al. (1988)	Tokioka et al. (1984)
NCAR	National Center for Atmospheric Research (USA)	CCM3	T42L18	Klehl et al. (1998)	Mass flux scheme (Zhang and McFarlane 1995)	Land surface model (Bonan 1998)	Slingo (1987), Klehl (1994)
SNU	Seoul National University (Korea)	SNU V.2	T31L20	Nakajima and Tanaka (1986)	Simplified RAS, diffusion-type shallow convection	Land surface model (Bonan 1998),	Le Treut and Li (1991)
SUNY	State University of New York (USA)	GLA GCM-01.0	4°_5°, L17	Harshvardhan et al. (1987)	Modified Arakawa-Schubert	Deardorff (1978)	Sud and Walker (1992)

this study, summer is defined as May through September (denoted: MJJAS), model data for the first summer (1997) contains all 30 pentads while model data for the second summer (1998) is limited to only the first 10 pentads.

This analysis framework for the model data provides 40 summertime pentads for 10 ensemble members for each model. This is approximately equal to 10–20 years of summertime data. The corresponding observational data period used for validation is based on 20 years of observed data, 1979 to 1998. Given that all the model simulations are based on the 1996–1998 period, raises the question of whether it is more appropriate to use observational data isolated to the same period or use a climatologically more representative period. Based on a number of modeling (Gualdi et al. 1999; Slingo et al. 1999; Waliser et al. 2001) and observational studies (Hendon et al. 1999; Sperber et al. 2000), it is believed that large-scale interannual SST variations appear to play very little role in determining the overall level of intraseasonal activity. On the other hand, it has been shown that El Nino – Southern Oscillation (ENSO) related variations do modulate the amount of spatial variability of the activity primarily through enhancing (diminishing) the activity in or near the central Pacific during El Nino (La Nina) periods. This is demonstrated by Fig. 2 that depicts the standard deviation of filtered observed rainfall for NH summer (left) and winter (hereafter NDJFM; right) using five different time periods. It is evident that the overall level of activity in the tropics does not change drastically from one decade (1979–1988) to another (1989–1998), or even from El Nino to La Nina periods. As mentioned above, the main interannual modulation appears to occur in the central Pacific Ocean region in response to (ENSO) variability in SST, although when considering the 1997/98 El Nino alone (3rd row) there appears to be a considerable increase (decrease) in variability over the eastern equatorial Indian Ocean during NH summer (winter).

3 Results

3.1 Generalized intraseasonal variability

To illustrate the general characteristics of ISV simulated by the AGCMs under study, Fig. 3 shows the standard deviations of filtered rainfall for NH summer from the observations and the ten participating models. In terms of the overall magnitude of the rainfall variability, at least four of the models considerably underestimate the variability (i.e., DNM, MRI, NCAR, SNU), with a fair number of the remaining models tending to overestimate the variability. In some cases, the models exhibit variability that is greater than the observations by nearly a factor of two in some isolated locations (e.g., COLA, GFDL, IAP, SUNY).

Closer examination of the spatial patterns of ISV reveals that the model patterns in the NH are fairly reasonable. In some cases, even the locations of the four peaks in the observed variability that appear in the NH (~70°E, 90°E, 110°E, and 130°E) tend to be faithfully represented (e.g., COLA, GEOS, IITM, SNU, and SUNY). The main exceptions to this are that the model peaks at 90°E lie slightly northward of the observed location, and they do not extend southward as far as the observed peak. In addition, the peak at 130°E in the COLA, GEOS, IITM and SNU models do not extend as far south as the observed peak, and the peak in the SUNY model extends too far east. There appears to be more difficulty in properly representing ISV near and south of the equator. For example, the COLA, GEOS, IITM and SNU models each have a peak in ISV at 60°E in the southern (~5–10°S) Indian Ocean which is not exhibited in the observations. Moreover, the observations exhibit a tongue of variability extending southward from the peak of variability over the Bay of Bengal (~90°E) that almost none of the models exhibit, except for possibly the SUNY model. It should also be noted that several of the models (GFDL, IAP, MRI, NCAR and SUNY) exhibit a relatively high amount of ISV in the central/western Pacific. Given that the sampling of the NH summer condition is biased towards the El Nino summer of 1997 (see Sect. 2), this feature does indicate an added measure of realism in the models. However, in comparing these maps to those in Fig. 2 (i.e., Fig. 2a, c, d), it appears the amount of variability in this region for the GFDL, IAP and SUNY models appears excessively high.

While our focus is on the NH summer ISV, it is instructive to also examine how the models portray the NH winter ISV. For example, even though there is some similarity between the summer and winter forms of ISV, their dominant modal characteristics appear to be quite different. This includes their propagation structure, interaction with the mean flow, underlying dynamics, etc. (e.g., Wang and Rui 1990; Hendon and Salby 1994; Hayashi and Golder 1997; Wang and Xie 1997). Thus it is instructive to examine the degree of consistency in the model representations of these two forms of ISV.

Figure 4 is the same as Fig. 3, but for NH winter ISV. For this case, many of the same generalities apparent in the NH summer ISV still hold. For example, the models that have high (low) NH summer variability tend to have high (low) NH winter variability. However, the overestimates of ISV for the winter case do not appear to be quite as high as for the summer case. Also, the same models that tended to produce a reasonable spatial pattern of variability in the summer hemisphere for the NH summer case also tend to produce a reasonable summer hemisphere pattern for the NH winter case (COLA, GEOS, IITM SNU, and SUNY). Interestingly, the same four models from this group (i.e., COLA, GEOS, IITM and SNU) that exhibited an erroneous peak of variability during NH summer in the winter hemisphere (Indian Ocean in this case) also exhibit an erroneous peak of variability in the winter hemisphere for the NH winter case (in this case, in the western Pacific). In fact, there tends to be a stronger tendency for these models to exhibit a double-banded (or double ITCZ) structure of rainfall over the longitudes shown. Another consistency between the NH winter and summer cases is that most models tend to exhibit considerably less ISV over the maritime continent than over the surrounding ocean regions, a characteristic also evident in the observations. Exceptions to this are the GFLD, IAP and MRI models, none of which exhibit a relative minimum over the maritime region for either the NH winter or summer case.

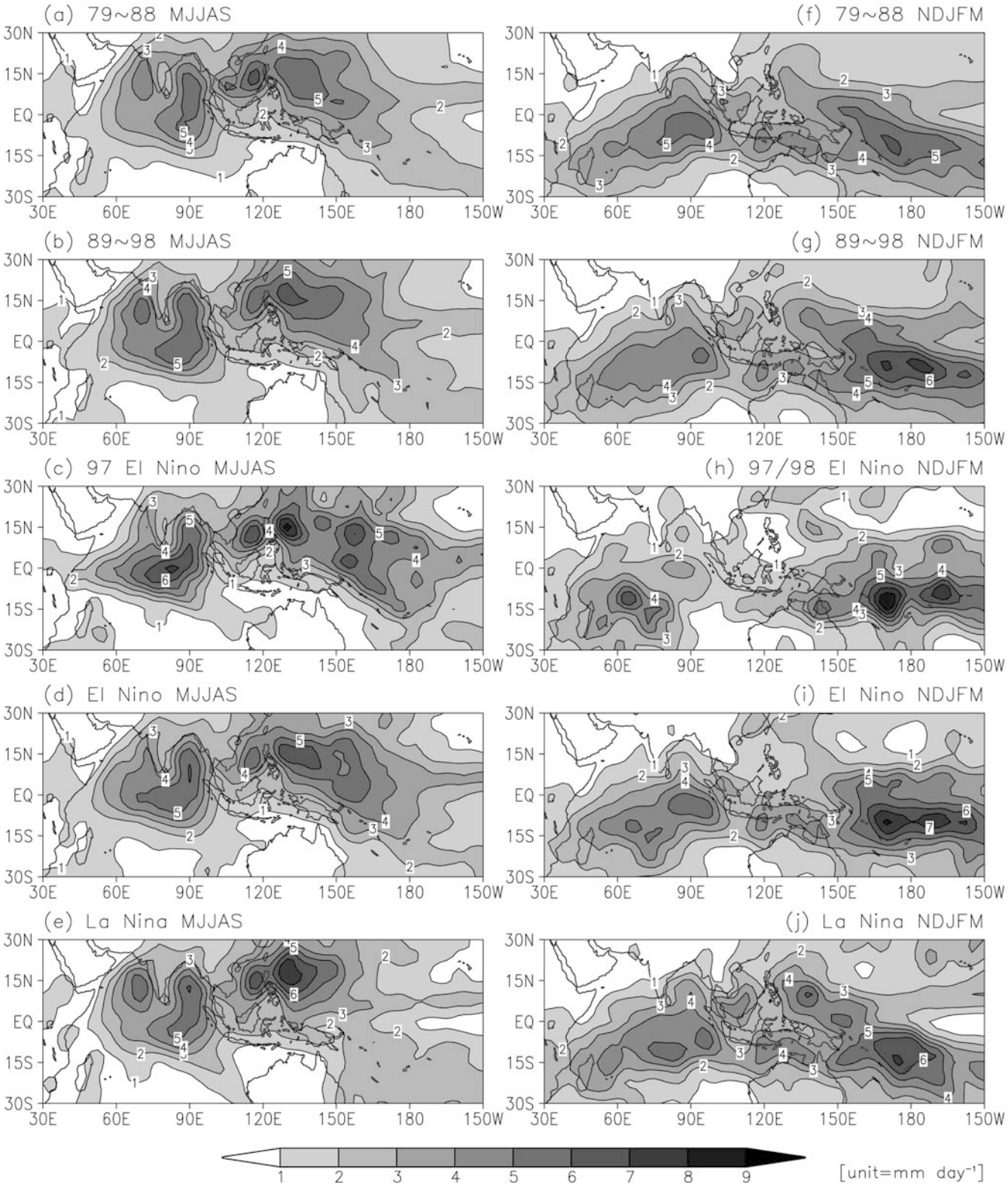

Fig. 2a–j Standard deviation of 20–90 day filtered rainfall (mm/day) for Northern Hemisphere summer (MJJAS; *left*) and winter (NDJFM; *right*) using four different time periods. **a, e** 1979 to 1988. **b, f** 1989 to 1998. **c, g** El Nino events between 1979 and 1998. **d, h** La Nina events between 1979 and 1998

Many of the findings described are summarized in Fig. 5, which shows a scatter plot of area-averaged summer versus winter ISV of rainfall. Most evident is the fact that as a general rule, strong (weak) NH wintertime area-averaged ISV implies strong (weak) NH summertime area-averaged ISV. In addition, independent of

season, there are three models that overestimate area-averaged ISV of rainfall by about 20% relative to the observed estimate, three models that have area-averaged ISV within about 10% of the observed estimate, and three models that underestimate area-averaged ISV of rainfall by about 25–30%, or considerably more in the case of DNM. While a model-data disagreement on the order of 25% may be reasonable given the uncertainties associated with the observed estimate itself, the absolute range amongst most (9 of 10) of the models (i.e. ~2.5–5 mm/day) does provoke concern. One positive conclusion that might be drawn from these results is that, to some extent, by rectifying model simulation shortcomings of ISV (e.g., too weak) in one season would likely lead to analogous improvements in the opposite season.

Figure 6 shows the relationship between area-averaged ISV of rainfall and VP200 for N.H. summer. For the most part, the relationship is as expected, more rainfall variability implies more VP200 (or divergent flow) variability. In fact, the relationship appears to be almost a linear one when considering at least 8 of the 10 models. However, there are two exceptions. The COLA model exhibits less VP200 variability than might be expected given its amount of rainfall variability and the relationship implied by the rest of the models. An even greater outlier is the IAP model, which exhibits a significantly greater amount of VP200 variability than would be expected given its amount of rainfall variability. It is not clear why these models exhibit such a different relationship between these two variables. Two model details that might be important in the case of the IAP model are that it has only nine vertical levels, nearly half or less the amount of most other AGCMs in the study, and it has prescribed clouds. However, it is not obvious how fewer model levels might lead to greater variability in the upper level divergent flow. Moreover, one would expect prescribed clouds to reduce the associated vertical velocity variability compared to interactive clouds due to the impact clouds have on the longwave radiation in the column. Additional model diagnostic information (e.g., radiation, clouds, diabatic heating profile) would be needed to determine the reason(s) for the above model differences.

3.2 Modal characteristics and northward propagation

In order to illustrate the space-time variability associated with each model's ISO, composite ISO events were computed. Events included in the composites were based on an extended empirical orthogonal function (EEOF) analysis that was performed on the filtered MJJAS rainfall data. The domain for the EEOF extended from 60°E to 180°, 30°N to 30°S, and includes –4 to +5 pentad lags (i.e., 10 lags). This EEOF procedure provides a way of isolating the principal modes of ISO space-time variability for the observations and the models. In the case of the models, there are 220 time-lagged instances of the rainfall analyzed (i.e. filtered MJJAS cases that include lags –4 to +5 pentads). The 30 filtered MJJAS pentads from 1997 accommodate 21 instances of a sliding 10-pentad lag window while the 10 filtered MJJAS pentads from 1998 can accommodate one. This makes 22 instances for each member of the ensemble, and thus 220 instances for all ten members. An analogous procedure was performed on the CMAP filtered precipitation data using 20 MJJAS periods (i.e., 1979–1998; in this case there were 420 time-lagged instances of the data). Once the first mode EEOF eigenvectors are identified, their associated amplitude time series can be used to select high amplitude events for compositing. In this case, pentad values of the time series that exceeded one standard deviation of the time series were used to select out lagged instances of the data (i.e., –4 to +5 pentads) for constructing the composites. These composites provide a way to succinctly present and compare the characteristics associated with the observed and models' principal modes of ISO variability, in particular their overall strength, fraction of filtered variability they account for, nature of the modes' northward propagation, etc. Note that since these composites were selected based on the EEOFs, they do have a fair amount of similarity to the underlying EEOF structure themselves (not shown). However, since they are composites based on the filtered data, they aren't constrained to only the variability associated with the single given EEOF mode.

The composite constructed based on the first EEOF mode of the CMAP data is illustrated in Fig. 7. This composite is based on the average of 38 events. For presentation purposes, the –4 and –3 lags, the –2 and –1 lags, the 0 and +1 lags, the +2 and +3, and the +4 and +5 lags have been averaged together. Note that the first EEOF mode used for constructing this composite accounts for 7.4% of the filtered variance. While this percentage seems low, the fact that this EEOF mode encompasses both space and time variability necessitates a reduction of variance that would not be found, for example, from a simple spatial EOF (in this case, the first mode from a standard spatial EOF analysis of filtered CMAP rainfall for the MJJAS period accounts for 13.4%). Evident from this figure is the very clear northeastward propagation of the convective signal that is typically oriented in a northwest–southeast direction. The data suggest that the time scale of this principal mode is about 40–50 days (e.g., Yasunari 1980; Lau and Chan 1986; Gadgil and Asha 1992). Note that through the cycle there is significant variability in convection in the equatorial Indian Ocean (e.g., Annamalai and Slingo 2001) but very little in the equatorial western Pacific. Keep in mind that the EEOF from CMAP, and thus the events chosen based on its amplitude time series, should not be necessarily biased toward any particular interannual state of the SST (See Sect. 2). Significant variability also extends from the Arabian Sea southeastward across southern India, across the Bay of Bengal, over northern portions of the maritime continent, and then

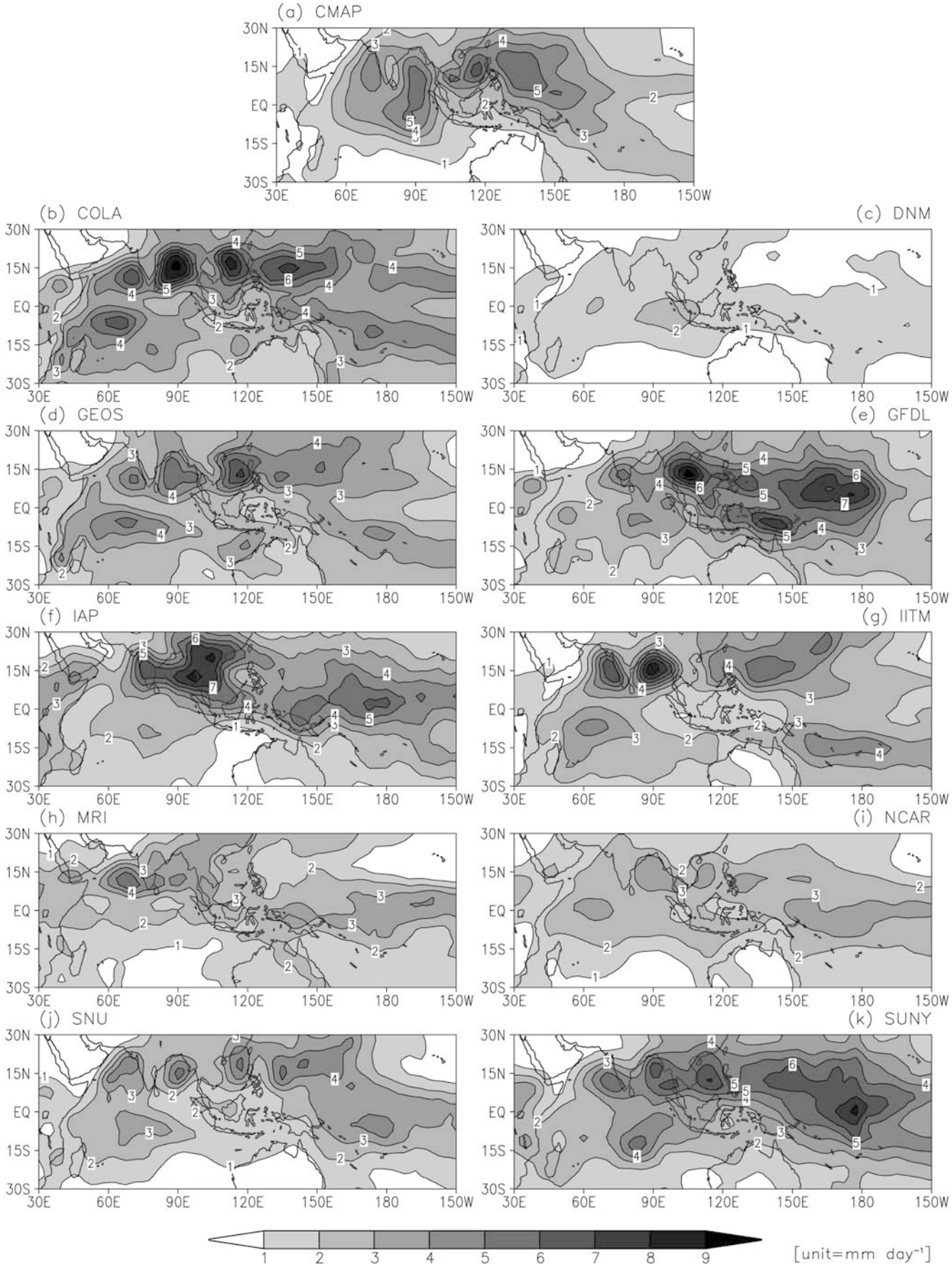
(a) CMAP
(b) COLA
(c) DNM
(d) GEOS
(e) GFDL
(f) IAP
(g) IITM
(h) MRI
(i) NCAR
(j) SNU
(k) SUNY
30N
15N
EQ
15S
30S
30E
60E
90E
120E
150E
180
150W
1
2
3
4
5
6
7
8
9
[unit=mm day⁻¹]

◀

Fig. 3a–k Standard deviation of 20–90 day filtered rainfall (mm/day) for Northern Hemisphere summer from the observations (*top*) for 1979 to 1998 and for the 10 participating AGCMs (lower). In the case of the models, there were 20 summer seasons of data, i.e. ten members each consisting of two years (see Sect. 2 for details of what constitutes a season)

across Southeast Asia and the northwest tropical Pacific Ocean.

In order to facilitate the comparison between the models' ISO composites and the CMAP case described above, the EEOFs for each of the models were first subject to a Procrustes targeted rotation (Richman 1986; Richman and Easterling 1988; Lucas et al. 2001). In this case, the target was the first EEOF mode of the CMAP data. For each of the models, a rotation was performed using the first three modes from each model. Put simply, a linear combination of the first three modes for a given model was produced that gave the best fit to the target, in this case the CMAP EEOF mode 1. The main reason for performing this rotation was that for a propagating cyclic disturbance such as the ISO, the principal modal structure is generally made up of two modes that are in quadrature (e.g., Murakami et al. 1986). However, the absolute phase of the two modes is arbitrary. Having each model's principal EEOF in an arbitrary phase in terms of its ISO makes the comparison between the models and between the models and observations more difficult. By performing these rotation, each model's principal EEOF will tend to have a phase that is roughly the same as the CMAP (i.e., target) EEOF. The addition of the third model mode to the rotation was simply to add other low-order variability to the rotation and thus possibly improve the model's chance of comparing well with the observations. However, the conclusions drawn from this portion of the analysis are not dependent on keeping this mode in the rotation.

The top bar chart in Fig. 8 shows the variances for the first three unrotated EEOF modes from the CMAP and model data. Also included in the figure is the variance associated with the first rotated EEOF (REEOF) mode from each of the models. The bottom bar chart in Fig. 8 shows the same information, except in terms of percentage of filtered variance captured by the modes. As expected, most of the EEOF 1 and 2 modes show up with similar variances, and thus as mentioned exist as a pair of modes that accommodate a propagating, cyclic disturbance. Also, in most cases the variance associated with mode three is considerably smaller than the variance associated with the first two modes. Consistent with Figs. 3 and 5, the variances associated with the models' principal EEOF modes display a fair range of values about the observed estimate 0.6 $(\mathrm{mm/day})^2$. In this case, the range extends from a high of about 1.0 $(\mathrm{mm/day})^2$ to a low of about 0.1 $(\mathrm{mm/day})^2$. However, it is worthwhile pointing out that in terms of percentage of NH summer ISV captured by the models' first two modes, they all fall within the range of about 5–8%, which is relatively close to the EEOFs from the observations. Figure 9 shows that this result is in rather stark contrast to the NH winter when the models appear to have considerably greater difficulty organizing ISV into coherent (i.e., MJO) modes to the same degree ISV is organized in the observations. For the latter, the percentage of ISV captured by the first EEOF is about 7.5% while for the models this value is anywhere between about 2.5 to 5%. Note that in regards to these percentages, application of the Preisendorfer N-rule significance test (Preisendorfer et al. 1981), as outlined in Lucas et al. (2001, see their Appendix) shows that the first EEOF modes presented are statistically significant at the 99% level. Finally, with respect to the models' REEOF percentage values given in Fig. 8, the main characteristic to point out is that they are very comparable to the values of the first two EEOF modes. This implies that these REEOF modes essentially capture the same type of variability exhibited in the first two modes but in a particular phase of the "cycle" and without much influence from the third EEOF mode.

The remaining panels of Fig. 7b–k, show the composites for each of the models. Note that the number of events in each composite is given in the caption, typically this is about 15. In this section, the focus of the discussion will be on the patterns of variability, including their propagating characteristics, rather than the strength of the variability which was discussed above (i.e. Figs. 3, 5, 8). Of the ten models, only a few exhibit a somewhat realistic northeastward propagating character (COLA, GEOS, GFDL, IAP and SUNY). However, none of the models demonstrate a great amount of fidelity in simulating all or most of the details of the spatial-temporal pattern well. For example, the COLA model exhibits a fairly reasonable spatial-temporal pattern over Southeast Asia and the western Pacific Ocean region. However, the variability is weak and disjointed over the maritime and Indian subcontinent regions, and consistent with Fig. 3, is almost non-exisitent in the central Indian Ocean. In fact, none of the models exhibit any systematic variability in the Indian Ocean in association with their ISO patterns. This is a major shortcoming of the model simulations, one that will be commented on further in Sect. 4, and in the next section, where it will be shown to have not only a local impact but also important downstream manifestations.

As indicated, there is a northward propagating component within the GOES ISO but the overall spatial extent of the variability is somewhat limited relative to the observations and the spatial scales of variability appear to be considerably smaller. As with the COLA model, the variability over the maritime and Indian subcontinent region is weak, even more so for the GEOS model. The ISO pattern associated with the SNU model exhibits many of the same strengths and shortcomings as the COLA and GEOS models discussed, falling somewhere in between in terms of realism. The GFDL model exhibits broad spatial scales of variability within its ISO pattern, scales that are somewhat consistent with the observed ISO pattern. Similar to the COLA and GEOS

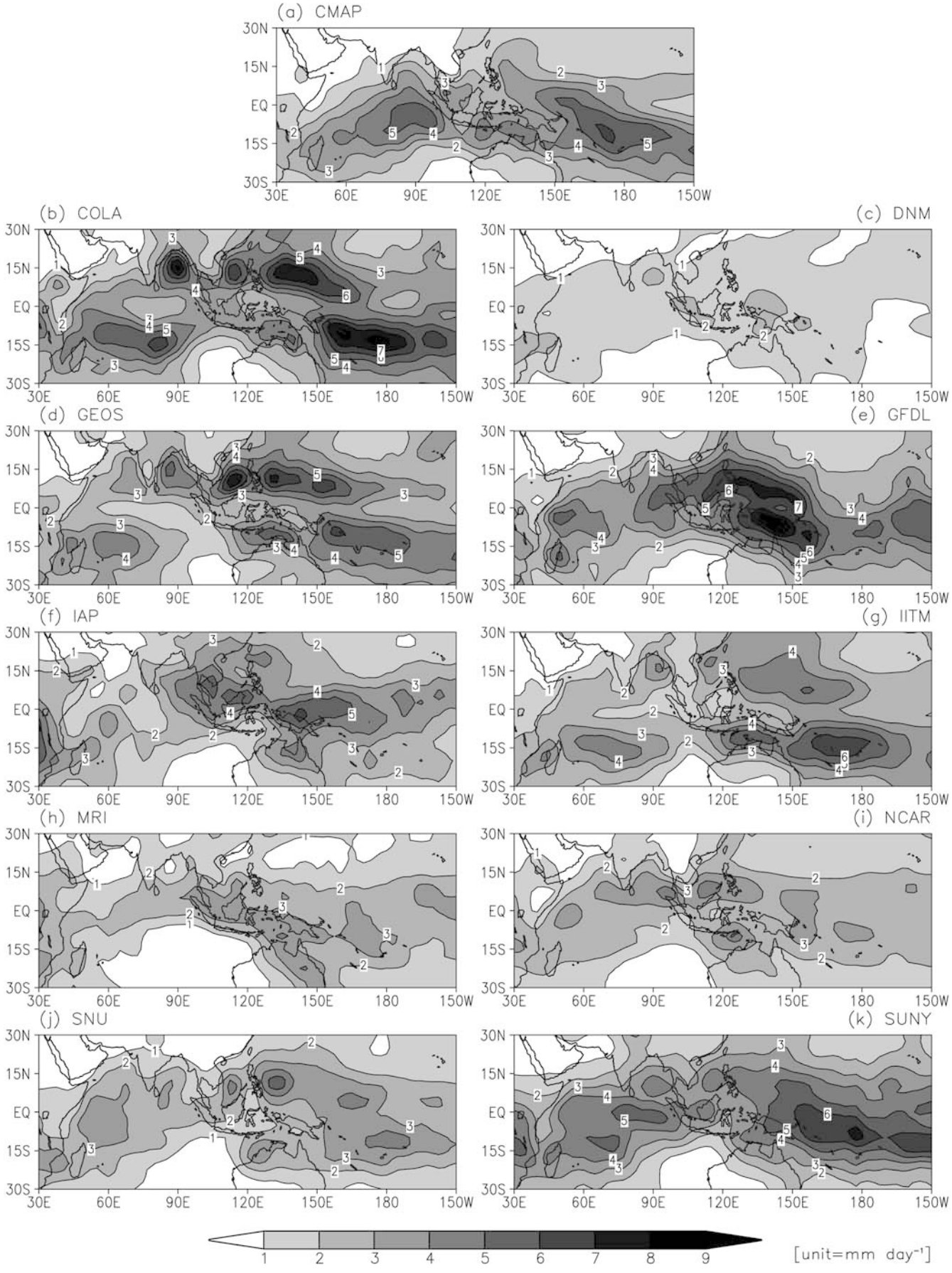
(a) CMAP
(b) COLA
(c) DNM
(d) GEOS
(e) GFDL
(f) IAP
(g) IITM
(h) MRI
(i) NCAR
(j) SNU
(k) SUNY
30N
15N
EQ
15S
30S
30E
60E
90E
120E
150E
180
150W
1
2
3
4
5
6
7
8
9
[unit=mm day⁻¹]

◀

Fig. 4a–k Same as Fig. 3, but for Northern Hemisphere winter

models, the variability around the Indian subcontinent is weak. However, in contrast to the COLA and GEOS models, there is a fair amount of variability over the maritime continent. To some extent this is also the case for the seasonal mean distribution of precipitation (Kang et al. 2002b). One curious feature regarding the GFDL composite is the rather strong variability over Southeast Asia and very little variability over the South China Sea, whereas the observations have just the opposite pattern. Similar to the models discussed, the SUNY model also exhibits weak and incoherent variability in the land regions that are effected by the ISO. Moreover, its ISO variability tends to be biased towards the warm interannual state of 1997 (see Fig. 2c, d) from which most of the MJJAS data was obtained. For example, Waliser et al. (2001) show the ISO EOF structure for the SUNY model for more generalized interannual SST conditions. The spatial pattern in that case is localized more around Southeast Asia than in the present case, although that study also showed how SST variability can bias the ISO rainfall variability toward/away from the central Pacific Ocean sector. Without similar sorts of information for the other models, it is unclear how much the interannual SST state of these model simulations may be influencing their ISO patterns (e.g., the GFDL model also exhibits considerable rainfall variability near the equatorial region of the dateline).

The IAP model exhibits a rather clear and robust northward propagating pattern. However, it is limited solely to the Indian subcontinent and Southeast Asian region, with little or no variability originating in the eastern equatorial Indian Ocean or extending into the western Pacific or over the maritime continent. Given the IAP's coarse spatial resolution (R15), it undoubtedly has a very different land mask and topography structure compared with most of the other models. This may be having a strong influence on the model's ISO variability. In contrast to most other models, the IITM and MRI models display a fair amount of variability around the Indian subcontinent region. In fact, the MRI model's variability is almost exclusively limited to this region. Both the IITM and NCAR model ISO patterns are more characteristic of standing rather than propagating oscillations. As with the lack of Indian Ocean variability, this is another feature that appears to be sensitive to ocean–atmosphere coupling (e.g., Kemball-Cook et al. 2002). Consistent with some of the models described, but considerably more so, the NCAR model exhibits almost no variability over land within its ISO pattern. This suggests that the model has very little intrinsic atmospheric ISV and it may be that the variability here is simply the atmospheric response to the ISV within the specified weekly SSTs (Wu et al. 2001). Finally, the DNM model exhibits very weak ISV, making it difficult to even define a coherent ISO pattern.

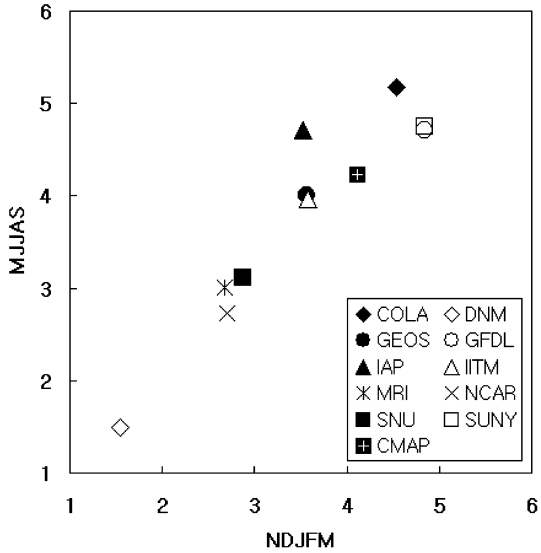

Fig. 5 Scatter plot of area-averaged variances, presented in terms of standard deviation, of 20–90 day filtered rainfall (mm/day) for NH summer (*vertical axis*) versus winter (*horizontal axis*). Data for summer and winter are taken from the domain 0°N–20°N, 60°E–150°E of Fig. 2 and from 5°N–15°S, 60°E–210°E of Fig. 3, respectively

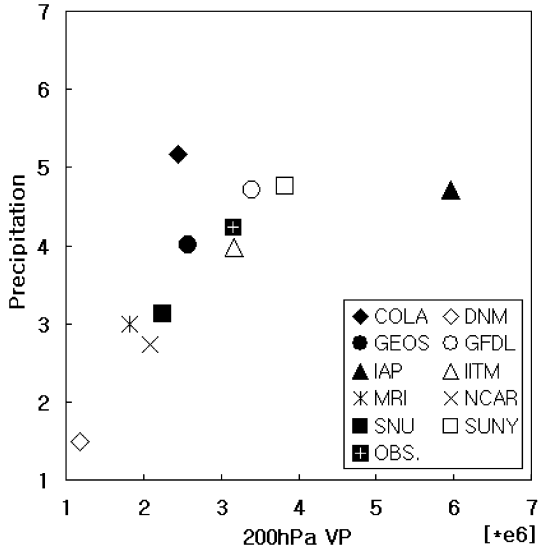

Fig. 6 Scatter plot of area-averaged variance, presented in terms of standard deviation, of 20–90 day filtered rainfall (mm day^{-1}) versus 200 hPa velocity potential (m^2 s^{-1}) for NH summer (MJJAS). Data for are taken from the domain 0°N–20°N, 60°E–150°E. Note the values associated with the *vertical axis* are the same as those in Fig. 5

3.3 Teleconnection properties

As mentioned in the Introduction, apart from the local influence that the ISO has on the tropical Indo-Pacific Ocean and Asian summer monsoon region, there are also considerable downstream influences that arise due to atmospheric teleconnections. These teleconnections induce ISV in the Americas, have an influence over

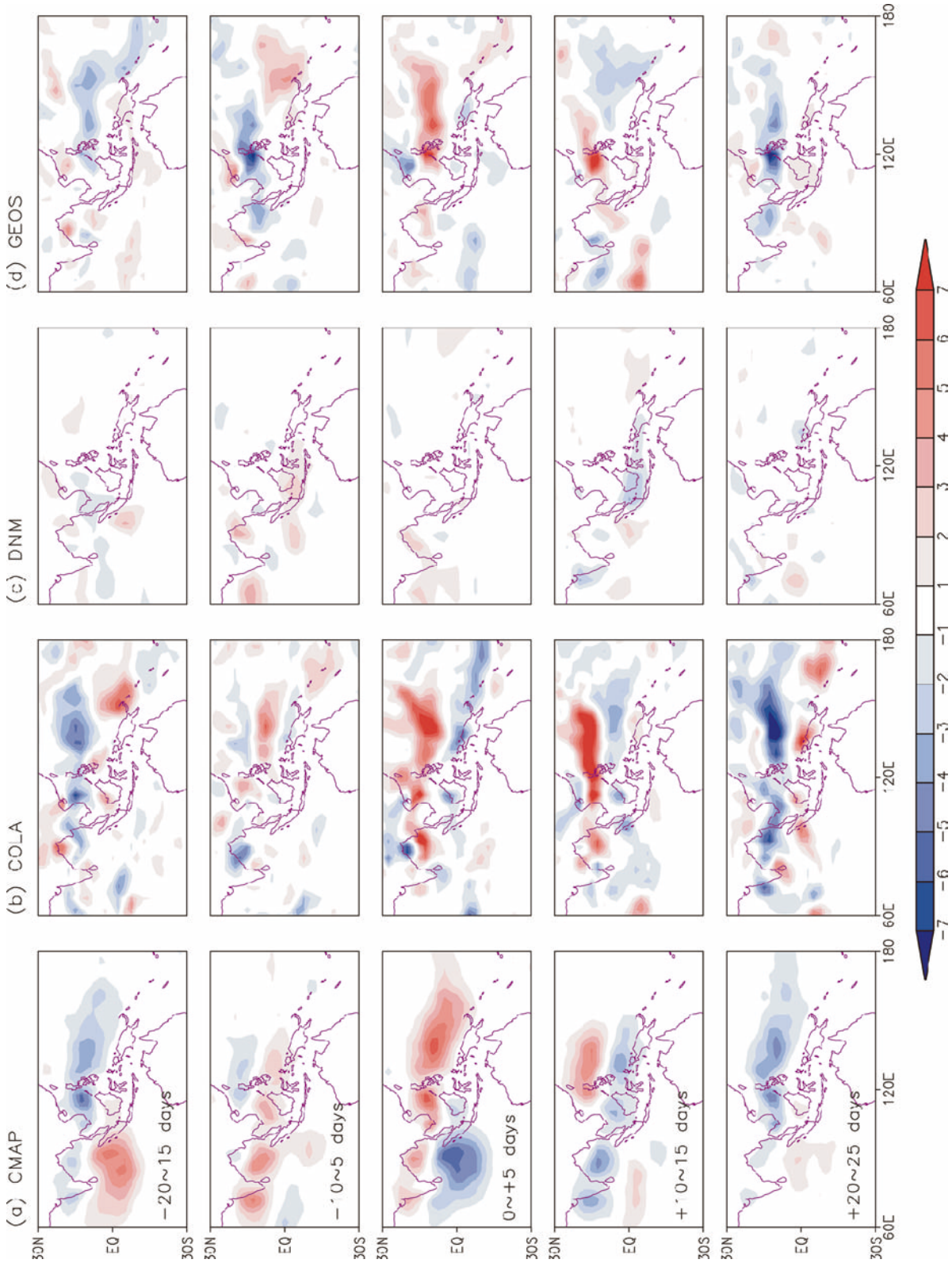
(a) CMAP
(b) COLA
(c) DNM
(d) GEOS
−20~15 days
−10~5 days
0~+5 days
+10~15 days
+20~25 days
30N
EQ
30S
60E
120E
180
−7
−6
−5
−4
−3
−2
−1
1
2
3
4
5
6
7

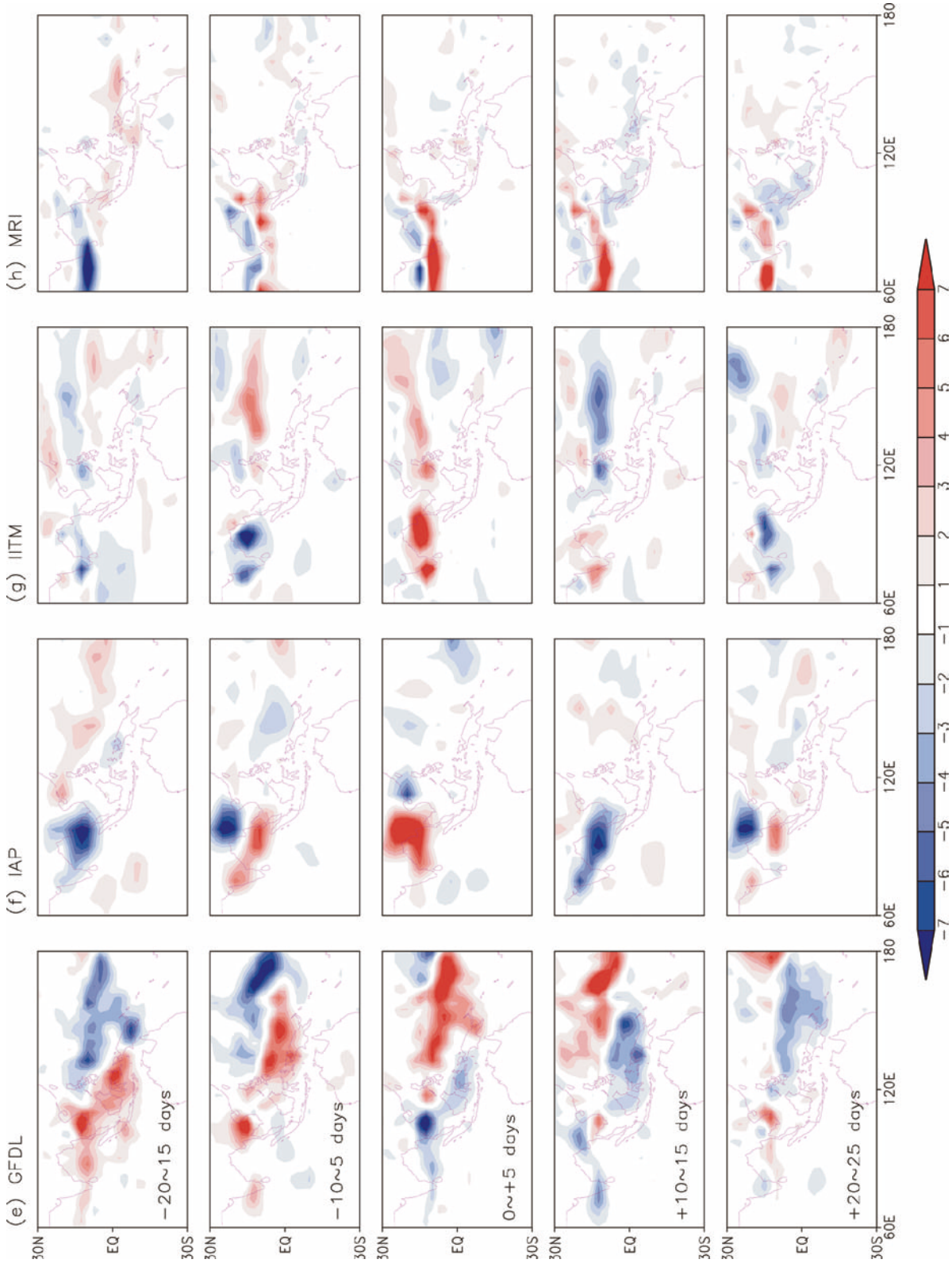

Fig. 7a–k Composite ISO events in terms of rainfall (mm/day) from observations (*left*) and participating models for the Northern Hemisphere summer. Construction is based on identifying events using an extended empirical orthogonal function (EEOF) analysis (see Sect. 3.2 for details). The number of events in each composite are given in the *parenthesis*: CMAP (38), COLA (12), DNM (10), GEOS (16), GFDL (11), IAP (18), IITM (16), MRI (18), NCAR (17), SNU (17), and SUNY (14)

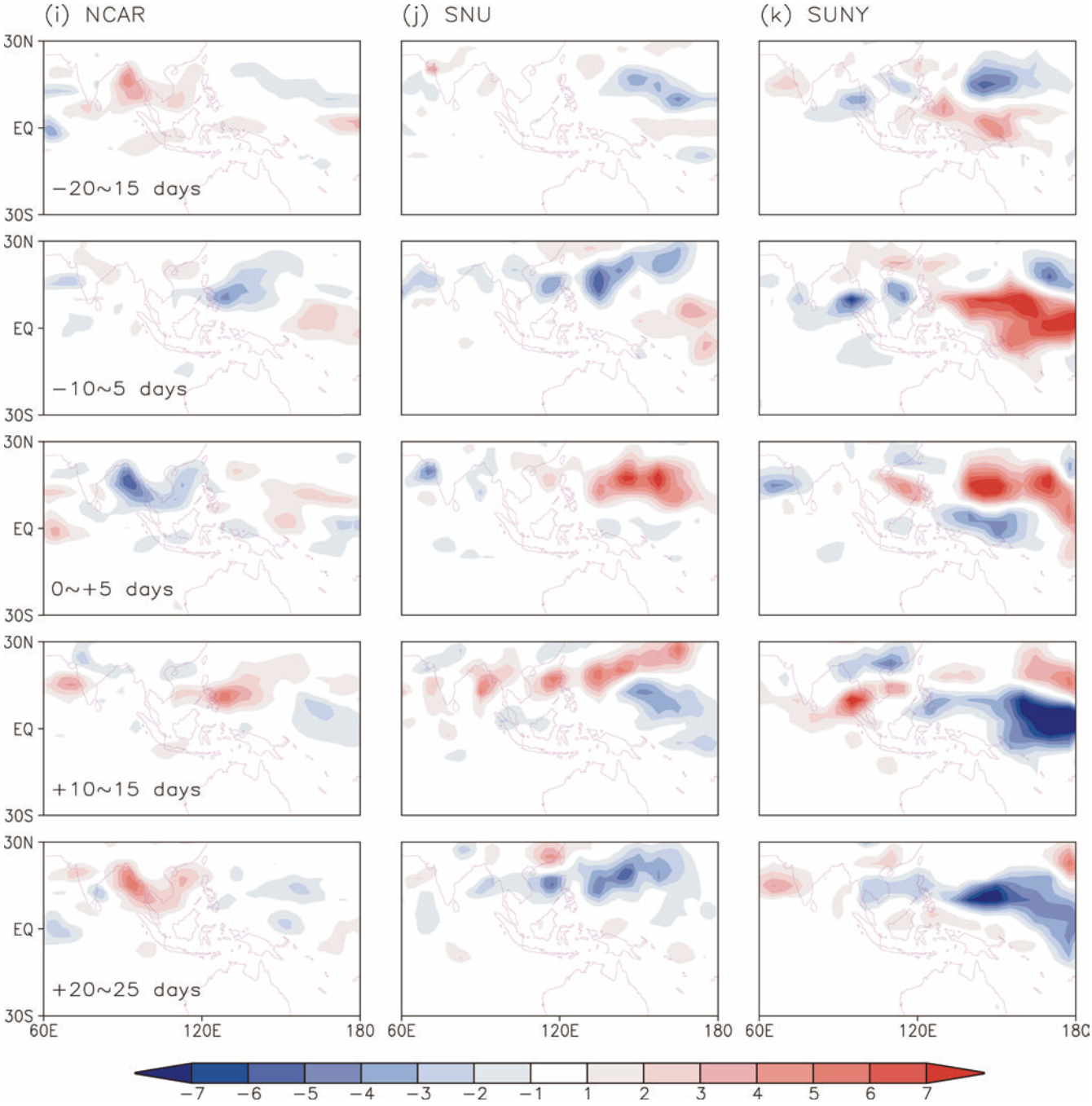

Fig. 7a–k (Contd.)

extreme precipitation events in these regions, and can even influence the development of tropical storms and hurricanes in the Pacific and Atlantic sectors during NH summer. They are linked to the strength and location of the tropical diabatic heat sources associated with the evolution of the ISO. While the previous section highlighted a number of shortcomings in regards to the modeled diabatic heating fields (represented in terms of precipitation), there was sufficient realism in a few cases to warrant an initial exploration of this issue. However, due to the significant inadequacies of most models' ISOs, as well as to limit the discussion, the figures associated with this part of the comparison will be limited to only three of the models. The choice of the three models to present was mainly dictated by the strength and spatial coherence of the rainfall pattern associated with each model's ISO (i.e., Fig. 8). Moreover, since the main diagnostic used in this part of the comparison is VP200, the models that also tended to have a component of its diabatic heat source on, or near, the equator were favored as well. This is because the divergent circulation is especially sensitive to near-equatorial heating and since the observed ISO exhibits relatively strong equatorial heating, (i.e., Fig. 7, leftmost panel) it is important

that this characteristic exist at least to some extent in order that the modeled VP200 composite resemble the observed.

Figure 10 shows the composite VP200 fields associated with the rainfall composites shown in Fig. 7 for the observations (leftmost panel), as well as the COLA, GFDL, and SUNY models. This particular form of VP200 composite is similar to that used by Higgins and Shi (2001) to demonstrate the observed influence of the ISO on the occurrence of hurricanes/typhoons. In that study, upper-level divergent (convergent) areas favored (suppressed) the development of tropical storms that turned into hurricanes. The observed VP200 ISO pattern is composed mostly of zonal wave number one variability. The entire pattern propagates east and the maximum and minimum have greater amplitudes in the Eastern versus the Western Hemisphere. While this latter characteristic is generally true of most of the three model composites displayed in Fig. 10, the models tend to exhibit higher zonal wave number variability, smaller meridional spatial scales, and generally have a less coherent structure.

Of the three model composites displayed in Fig. 10, the VP200 response of the COLA model tends to be weakest and least coherent. This arises due to the facts that the COLA equatorial heating/precipitation is weaker than observed and the heating that does exist at any given longitude tends to include both positive and negative centers which can have a cancellation effect on the large scales associated with VP200 variability. For example, examination of Fig. 7a shows that the observed ISO pattern at –20 to –15 days and 0 to +5 days exhibits almost a dipole heating pattern along the equator, with fairly large meridional scales (~20° latitude). Moreover, at –10 to –5 days and +10 to +15 days, there tends to be one strong heating center near the equator. Neither of these conditions typically held for the COLA model ISO pattern (Fig. 7b). The observed ISO rainfall pattern also exhibits a fairly well defined eastward component along with the northward propagation. This eastward propagation influences the eastward propagation of the VP200 anomalies. The COLA model exhibits very little eastward propagation of rainfall anomalies, being composed mostly of northward

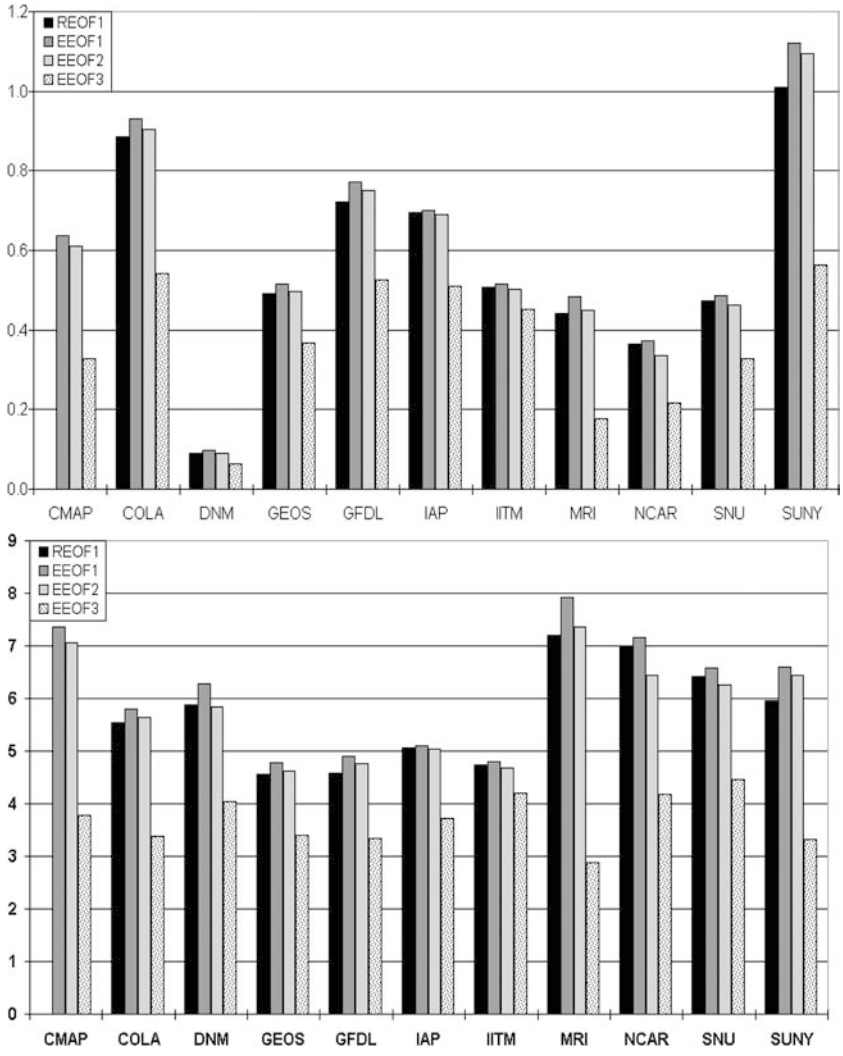

Fig. 8 (*Top*) Variance (mm^2 day^{-2}) of the first three extended EOF (EEOF) modes of NH summer filtered rainfall over the region 60°E to 180°, 30°N to 30°S and for –4 to +5 pentad lags (see Sect 3.2 for details) from the observations (i.e., CMAP) and the 10 participating models. In addition, the variance associated with the first rotated EEOF (REEOF) for each of the models is also shown. (*Bottom*) the same as the top bar chart, except in terms of percentage of filtered variance accounted for by each mode

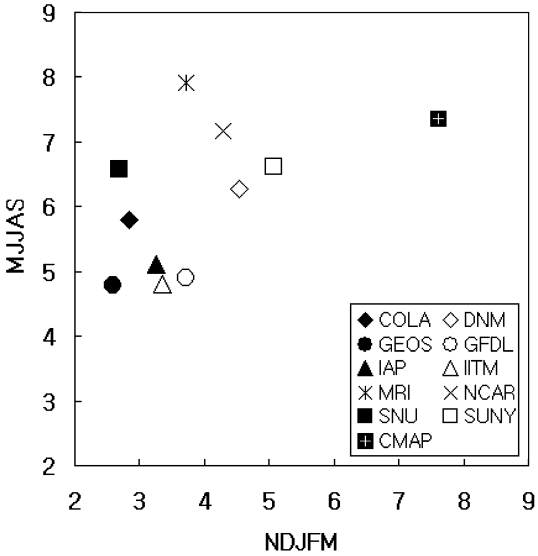

Fig. 9 Percentage of filtered variance accounted for by the first extended EOF (EEOF) of NH summer (*vertical axis*) versus NH winter (*horizontal axis*) filtered rainfall over the region 60°E to 180°, 30°N to 30°S and for –4 to +5 pentad lags (see Sect. 3.2 for details) from the observations (i.e. CMAP) and the 10 participating models

propagating bands of precipitation. This in turn makes the eastward propagation of the VP200 anomalies appear very weak and incoherent relative to the observations.

The GFDL VP200 composite is fairly realistic in terms of amplitude and spatial scales of variability, although the propagation speed appears to be slower than observations. Two characteristics are worth highlighting. The first is that consistent with this model's lack of strong heating (i.e., rainfall) variability in the equatorial Indian Ocean, the amplitude of the VP200 anomaly extending westward from the Indian Ocean around to the Atlantic is weaker than the observed pattern. In addition, there is a stronger suppression of VP200 variability within the ISO composite in the central and eastern Pacific Ocean relative to the observations. Each of these appear to act together to reduce the amount of ISV over the Eastern Hemisphere relative to the observations. The SUNY model exhibits the same problem with the lack of Indian Ocean heating variability and the ramifications this has on VP200 variability west of this region. In addition, like the COLA model, the SUNY model also displays smaller scales of zonal and meridional variability than the observed pattern. Although in contrast to the COLA model, there is a better-defined eastward propagation of the large-scale VP200 anomalies.

While this discussion has focused on only three of the ten models, examination of the other seven model VP200 composites showed similar, or often greater, shortcomings than the models just discussed. In addition to examining the tropical VP200 variability associated with the ISO rainfall composites shown in Fig. 7, Northern Hemisphere (0–60°N) 200 hPa eddy stream function (SF200) composites were also examined. While the observed SF200 composite showed a somewhat coherent SF200 zonal wave number one structure (+/–3 $m^2 s^{-1}$) propagating eastward in the latitude band 10–30°N, the model composites generally exhibited largely incoherent structures with much higher zonal wave number variability (~3–5). There was a signature of zonal wave number one variability with nearly realistic amplitude in the GFDL, IAP and SUNY models, however the degree of realism was not sufficient to present additional figures. It is likely that, along with the shortcomings of the models in terms of their ISO-related diabatic heating fields, the number of events included in the model ISO composites is simply insufficient to produce a robust signal. Future ISO intercomparison studies will likely need to produce significantly longer simulations and/or more ensemble members to adequately examine this issue.

3.4 ISO and monsoon predictability

To date, AGCMs have been singularly unsuccessful at even hindcasting seasonal monsoon anomalies with any skill (e.g., Sperber and Palmer 1996; AAMWG et al. 2001). However, the degree to which these forecasts suffer due to shortcomings in the models or as the result of the intrinsically unpredictable component of the monsoon is still not clear. In regards to the former, the results described certainly indicate that the models still exhibit significant problems in simulating at least the intraseasonal component of the monsoon. Determining how the intraseasonal time scale rectifies onto the seasonal time scale of the monsoon is still the subject of much research (e.g., Ferranti et al. 1997; Krishnamurthy and Shukla 2000; Sperber et al. 2000; Lawrence and Webster 2001). In regards to the latter aspect, a comparison of the relative sizes of intraseasonal versus interannual monsoon rainfall variability (e.g., Fig. 1), along with the relative insensitivity of the former to interannual SST variations, suggests that at least part of the unpredictable component of seasonal monsoon rainfall is due to the stochastic nature of the ISO (e.g., Sperber et al. 2000; Waliser et al. 2001). This begs the question of what considerations should be made in regards to the ISO when assessing monsoon predictability from GCM experiments. The model simulations in this CLIVAR study provide the means to at least consider how the strength of a model's ISO might influence the model's seasonal monsoon variability, and thus impact its estimate of monsoon predictability.

Figure 11 shows a scatter plot of the strength of each model's NH summer ISO in terms of the standard deviation of filtered rainfall variability versus each model's intra-ensemble standard deviation of seasonal mean (JJA) rainfall anomalies. The former is the same quantity plotted on the vertical axis of Fig. 5 and gives a

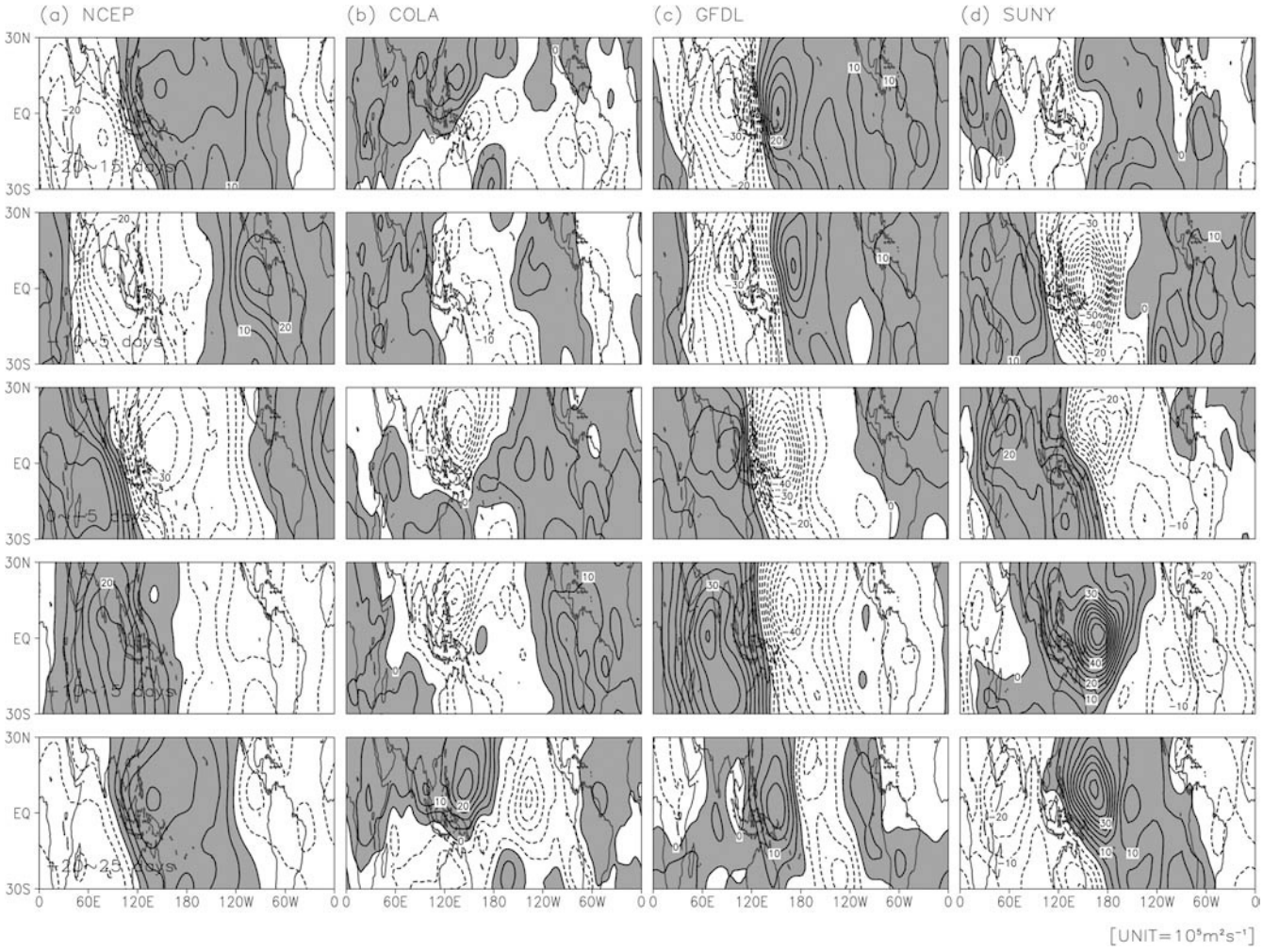

Fig. 10a–d Same as Fig. 7, but for VP200 and only for a select number of models

measure of the strength of the ISO within each model [qualitatively similar results are found if the variance of the first EEOF of ISO rainfall (i.e. Fig. 8) is used instead]. The latter quantity was determined by computing the seasonal (JJA) mean anomalous rainfall separately for each summer period of the model ensemble (2 years * 10 members = 20 summer periods). The intra-ensemble variance was then computed for each year and then the two years (1997, 1998) were averaged together. From this map, the domain-averaged (0°N–20°N, 60°E–150°E) variances were computed and then the result plotted in terms of the standard deviation. This latter quantity provides a measure of intra-ensemble variability associated with a model hindcast of the seasonal mean monsoon anomaly given SSTs specified from observations. Since a larger standard deviation suggests less predictable seasonal monsoon anomalies and vice versa, this measure provides a qualitative indication of the predictability of the monsoon as estimated by the given model. The observational analog to the ISO strength is the same as that plotted in Fig. 5, while the analog for the monsoon variability is simply the domain-averaged interannual rainfall variability computed using the CMAP data.

The figure shows a clear relationship in which a stronger (weaker) ISO is associated with greater (smaller) intra-ensemble monsoon variability. This relationship might arise from two considerations of the monsoon system. First, as indicated, ISO-related fluctuations would be expected to influence the seasonal mean intra-ensemble variability due to their relatively large amplitude and stochastic, non-periodic nature (e.g., Fig. 1). Note that during NH summer and over the Indian/Southeast Asian sector, the observed interannual rainfall variance is only about 40% of the size of the intraseasonal rainfall variance. Second, it is likely that both of these quantities are inherently tied to the strength of the models' hydrological cycles, and thus enhancing the hydrological cycle of a given model would increase both quantities plotted. For example, a stronger annual cycle in monsoon rainfall would naturally lead to larger variations in seasonal-mean monsoon rainfall (i.e., variance in rainfall is typically high when/where the mean is high). This aspect is demonstrated in Fig. 12.

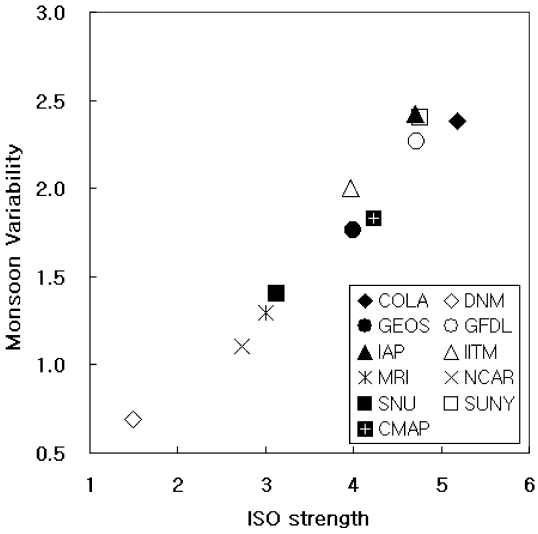

Fig. 11 Scatter plot of area-averaged variance, presented in terms of standard deviations, of 20–90 day filtered rainfall (mm/day) for NH summer (*horizontal axis*) versus intra-ensemble standard deviation of NH summer rainfall variability (*vertical axis*). Data are taken from the domain 0°N–20°N, 60°E–150°E. The data associated with the *horizontal axis* are the same as the data for the *vertical axis* in Fig. 4

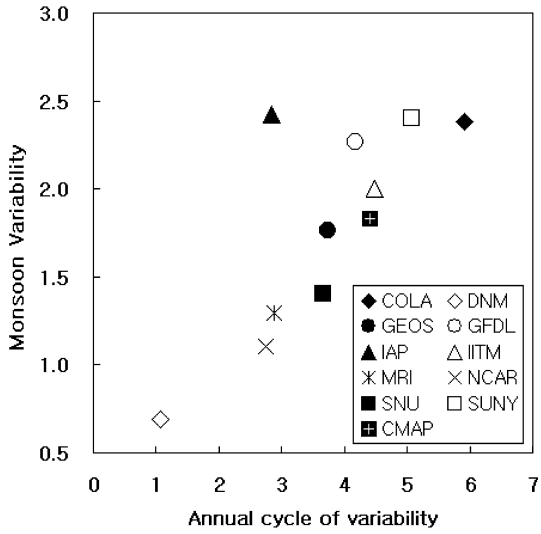

Fig. 12 Scatter plot of area-averaged annual cycle strength of rainfall (mm/day) for NH Asian monsoon sector (*horizontal axis*) versus intra-ensemble standard deviation of NH summer rainfall variability (*vertical axis*). Annual cycle is obtained from 20-year (1979∼1998) climatological mean summer (June to August) minus mean winter (December to February) rainfall. Data are taken from the domain 0°N–20°N, 60°E–150°E. The data associated with the *vertical axis* are the same as the data for the *vertical axis* in Fig. 11

While this relationship is not quite as robust as that in Fig. 11, it still emphasizes that the strength of a model's annual cycle of monsoon rainfall influences its intra-ensemble variability in a manner one might expect from simple statistical considerations. Further, when Figs. 11 and 12 are considered together, they also demonstrate that the strength of a model's annual cycle and ISO tend to go hand in hand. Thus from these plots, it is not clear to what degree the relationship shown in Fig. 11 stems from ISO activity versus the overall strength of a model's hydrological cycle.

Quantifying the contributions from these two processes to the relationship shown in Fig. 11 is not easy. One might suspect that the component associated with the different models' hydrological strengths could be removed by calculating the same quantities shown in Fig. 11 from a larger multi-year, multi-member ensemble for one or more models separately. In this case, the ensemble-average ISO strength for each year would be plotted against the intra-ensemble variability of the seasonal mean rainfall for the given model. However, for a large ensemble, one that would depict a statistically significant measure of intra-ensemble variability, there is a likelihood that the ensemble-average ISO strength (i.e., overall ISO activity level, not its spatial or modal reorganization) would tend towards the same value for each year given its insensitivity to large-scale interannual SST anomalies. Thus even though the strength of a model's ISO activity might indeed be influencing the intra-ensemble variability of the monsoon, it might in fact be hard to detect by this approach. At present there is too little information regarding the influence of interannual SST anomalies on N.H. summer ISO activity to really assess if the outcome indicated for this type of experiment would indeed prevail. The model study by Waliser et al. (2001) indicated very little impact of interannual SST anomalies on NH summer (or winter) ISO activity. Similar, results were found for NH winter ISO activity in the studies by Slingo et al. (1999) and Gualdi et al. (1999). While the latter of these studies did find that a small but statistically significant impact did exist in their model ensemble, its detection was quite sensitive to the ensemble size used. The paucity of studies in this area, coupled with the obvious shortcomings that models have in simulating the ISO, strongly suggest that better models and more research is needed to resolve this issue. In summary however, the relationship shown in Fig. 11 is likely to continue to hold for any set of GCMs. Taken at face value, this relationship indicates that GCM estimates of monsoon predictability should be considered in light of the strength of the model's ISO variability.

4 Summary and discussion

Our purpose is to present results from the Asian–Australian Monsoon GCM Intercomparison Project with a focus on the intraseasonal variability (ISV) associated with the Asian summer monsoon. The analysis is based on 10-member ensembles of two-year simulations from 10 different AGCMs. The AGCM simulations used here are from COLA (USA), DNM (Russia), GSFC (GEOS, USA), SUNY (GLA, USA), GFDL (USA), IAP (China), IITM (India), MRI (Japan), NCAR (USA), and SNU (Korea). The main objective was to summarize the systematic successes and errors that are common to

present-day AGCMs in simulating ISV associated with the Asian summer monsoon, namely in the form of the Intraseasonal Oscillation (ISO), along with its connections to other components of the weather/climate system.

An assessment of the overall magnitude of intraseasonal variability (ISV) of rainfall during N.H. summer (MJJAS) shows (Figs. 3, 5) that four of the ten models considerably underestimate the variability (DNM, MRI, NCAR, SNU), with about the same number tending to overestimate the variability (COLA, GFDL, IAP, SUNY). When averaged over the northern Indian Ocean/Southeast Asian sector, the model-data disagreement of ISV of rainfall ranges between about +/– 25% of the observed. However, in isolated locations the disagreement can range up to +/– 100%. While this level and range of disagreement raises considerable concern, there are some important details in the spatial structure of ISV of rainfall that are reproduced by a number of the models. For example, the observed pattern of ISV of rainfall exhibits four peaks at around 15°N at longitude of about 70°E, 90°E, 110°E, and 130°E. About half of the models produce reasonable approximations of this feature (COLA, GEOS, IITM, SNU, and SUNY). However, all the models have great difficulty in properly representing ISV of rainfall near and south of the equator. In particular, the observations exhibit a strong peak of variability at the equator between about 80°E and 100°E that extends southward from the Bay of Bengal. Except for one or two exceptions, none of the models are able to reproduce this feature to any extent. Rather, in a few models, an erroneous peak of variability occurs west of 60°E in the southern (~5–10°S) Indian Ocean (COLA, GEOS, IITM and SNU). This latter feature appears to come from a propensity to form double convergence zones about the equator.

While the focus of the study is on the NH summer ISV, some analysis was performed to compare the models' simulation quality of NH winter and summer ISV. In general it was found that the models that have high (low) NH summer ISV tend to have high (low) NH winter ISV. Also, the same models that tended to produce a reasonable spatial pattern of variability in the summer hemisphere for NH summer also tend to produce a reasonable summer hemisphere pattern for NH winter. In addition, the tendency for producing a double tropical convergence zone was exhibited in N.H. winter in the same models that exhibited it in NH summer, giving way to erroneous peaks in ISV of rainfall along 10–15°N. Another consistency between the N.H. winter and summer ISV representations is that most models tend to exhibit considerably less ISV over the maritime continent than over the surrounding ocean regions, a characteristic also evident in the observations. Exceptions to this are the GFDL, IAP, and MRI models, none of which exhibit a relative minimum over the maritime region for either the NH winter or summer case. One positive conclusion that might be drawn from the above findings is that, to some extent, rectifying model simulation shortcomings of ISV (e.g., too weak, double convergence areas) in one season would likely lead to analogous improvements in the opposite season. This conclusion is only true to the extent that the same mechanistic processes underlie summer and winter ISOs.

Along with analysis of ISV in general, the models' principal spatial-temporal structure of ISV was examined via an extended EOF (EEOF) analysis. This procedure provided the means to capture what would be deemed each model's ISO pattern that is associated with its depiction of the Asian summer monsoon and compare these patterns to observations (Figs. 7, 8). The observed EEOF pattern exhibits a localized precipitation region that initiates in the equatorial Indian Ocean and then propagates both north and east. The precipitation region spreads out into a northwest-southeast oriented band that impacts India, the maritime continent, Southeast Asia and the equatorial western/northwestern tropical Pacific Ocean. Of the ten models, only a few exhibit a somewhat realistic northeastward propagating character. These include the COLA, GEOS, GFDL, IAP and SUNY. However, none of the models demonstrate a great amount of fidelity in simulating all or most of the details of the spatial-temporal pattern well. For example, none of the models exhibit any systematic variability in the Indian Ocean in association with their ISO patterns. This would appear to be a major shortcoming of the model simulations and warrants a number of comments. First, since this region might be considered the genesis region for ISO convective anomalies, the lack of variability in this region might at least partially explain the weak ISO character of many of the models. Second, the tendency of some models to organize convection off the equator in the form of double convergence zones may certainly play a degrading role in terms of properly representing the convection in this phase of the ISO. Third, there is some evidence that coupled air-sea processes might be important in this region for initiating, enhancing and/or maintaining ISO-related convection (e.g., Waliser et al. 1999a; Kemball-Cook and Wang 2001; Fu et al. 2002; Kemball-Cook et al. 2002). In fact, since the models were forced with weekly SST, the uncoupled nature of the intraseasonal SST forcing could even have a degrading impact on the ISO simulations in some case where the SST and ISO variability were not properly phased (Wu et al. 2001). Fourth, and as highlighted later, the manifestations of this shortcoming are not limited to the local area (i.e., Indian Ocean) but have downstream/extra-tropical impacts as well.

A few items are encouraging to note. As already mentioned, a number of models do have some semblance of a northeastward propagating ISO mode. However, along with the Indian Ocean problem mentioned, the model ISOs typically suffer from one or both of the following features: (1) the rainfall band(s) are too zonal and thus lack a clear eastward

propagating component; (2) the zonal and/or meridional spatial scales of the rain band(s) are too narrow and thus for example either India or the western Pacific Ocean often do not exhibit variability within the mode. Another encouraging aspect is that the percentage of variance captured by a number of models' principal EEOF modes of NH summer ISO variability are in better agreement with the observed percentage than for the case of NH winter ISO variability (Fig. 9). In the latter case, all the models' principal EEOF mode captures considerably less variance than the variance within the principal EEOF mode of the observations. Finally, consistent with observations, most of the models appear to exhibit less ISV/ISO variability over the land regions associated with the Asian and Maritime continents than the nearby ocean regions.

A limited assessment was made of the models' representation of the large-scale teleconnection links associated with the ISO using a composite analysis of the VP200 and SF200. For the most part, these teleconnection representations are most hampered by the weak and/or incoherent nature of the models' spatial-temporal patterns of ISO rainfall. Even when considering the "better" models in this regard, the proper representation of a number of detailed features appears to be important. In particular the strength and evolution of equatorial heating appears particularly important, with the lack of variability in the equatorial Indian Ocean, that is found in all the models, being especially problematic.

Analysis of the model ensembles showed a positive relationship between a model's ISO strength and its intra-ensemble variability of seasonal mean rainfall (Fig. 11). Apart from the caveats discussed in Sect. 3.4, this relationship suggests that part of the unpredictable nature of the Asian summer monsoon may stem from the relatively large-amplitude, stochastic nature of the ISO. While this has direct implications on seasonal mean monsoon forecasting as well as on determining the limits of predictability from GCM simulations, it raises two other considerations worth discussion. First, given the great difficulty associated with seasonal mean monsoon forecasting, albeit which may in part be derived from the ISO, it may be more productive to pursue deterministic forecasts of the ISO's themselves rather than predictions of the lower-frequency fluctuations (e.g., seasonal departures). Evidence from both statistical models (Waliser et al. 1999b; Lo and Hendon 2000; Mo 2001; Wheeler and Weickmann 2001) and twin-predictability experiments (Waliser et al. 2003a,b) suggest that ISO fluctuations may be predictable with useful skill at lead times of about 20 days or more. Even without the means to predict seasonal anomalies a number of months in advance, such ISO forecasts would have tremendous benefit in terms of helping to foreshadow onset and break periods of the monsoon.

The second consideration concerns the implication of this result has on the low-frequency characteristics of monsoon predictability. As mentioned earlier, global-scale ISO activity exhibits fairly pronounced interannual variability and there appears to be only weak associations with interannual SST anomalies (see Introduction and Sect. 3.4). This implies that these interannual variations in ISO activity may be internally generated. In contrast to the interannual time scale, there does appear to be a link between interdecadel variations in global scale ISO activity and interdecadal anomalies in SST. Using analyzed data sets, Slingo et al. (1999) showed that ISO variability, as well as Indian Ocean SST, have increased over the last two decades, and in fact was able to reproduce the trend in ISO variability with an AGCM forced with observed SSTs. Coupled with the unpredictable nature that ISO activity has on interannual time scales, this secular variation in ISO activity may be playing a role in the varying relationship between Asian summer monsoon anomalies and related quantities/predictors (e.g., ENSO). These interdecadal variations in ISO activity need to be more fully understood, particularly their generating mechanisms and the role they may play in the secular variations of monsoon predictability (e.g., Parthasarathy et al. 1991; Hastenrath and Greischar 1993; Kumar et al. 1999).

Finally, while the studies by Kang et al. (2002a, b) examined in some detail the quality of the seasonal mean and interannual anomalous rainfall characteristics associated with these AGCM ensemble simulations, it is instructive to consider these results in light of their implications for the simulation of seasonal mean rainfall. Figure 13 shows the seasonal (MJJAS) mean rainfall from the observations (top two panels) and from each of the models averaged over both the 1997 and 1998 summers and all members of the ensembles. The poor representation of the mean rainfall in the equatorial Indian Ocean region is worth noting, specifically the weak and in some cases very weak mean precipitation produced by the models in the eastern equatorial Indian Ocean. In addition, a number of the models exhibit an erroneous double convergence zone structure about the equator. Both these features tend to mimic shortcomings that were found for the spatial structure of the models' intraseasonal variability (e.g., Fig. 3). Taking the viewpoint that the spatial structure of the mean precipitation pattern is determined by the spatial structure of the high-frequency transient variability suggests that the errors in these seasonal means arise, at least in part, from shortcomings in the intraseasonal variability –namely the models'ISO representations. Considerations such as this, along with the importance of the ISO for subseasonal prediction of monsoon variability, strongly warrant an unrelenting commitment to

Fig. 13a–i NH summer (MJJAS) seasonal mean rainfall (mm/day) from the observations for 1979 to 1998 (*top left*) and for 1997–98 (*top right*) and for the 10 participating AGCMs (*lower*). In the case of the models, there were 20 summer seasons of data, i.e. 10 members each consisting of two years

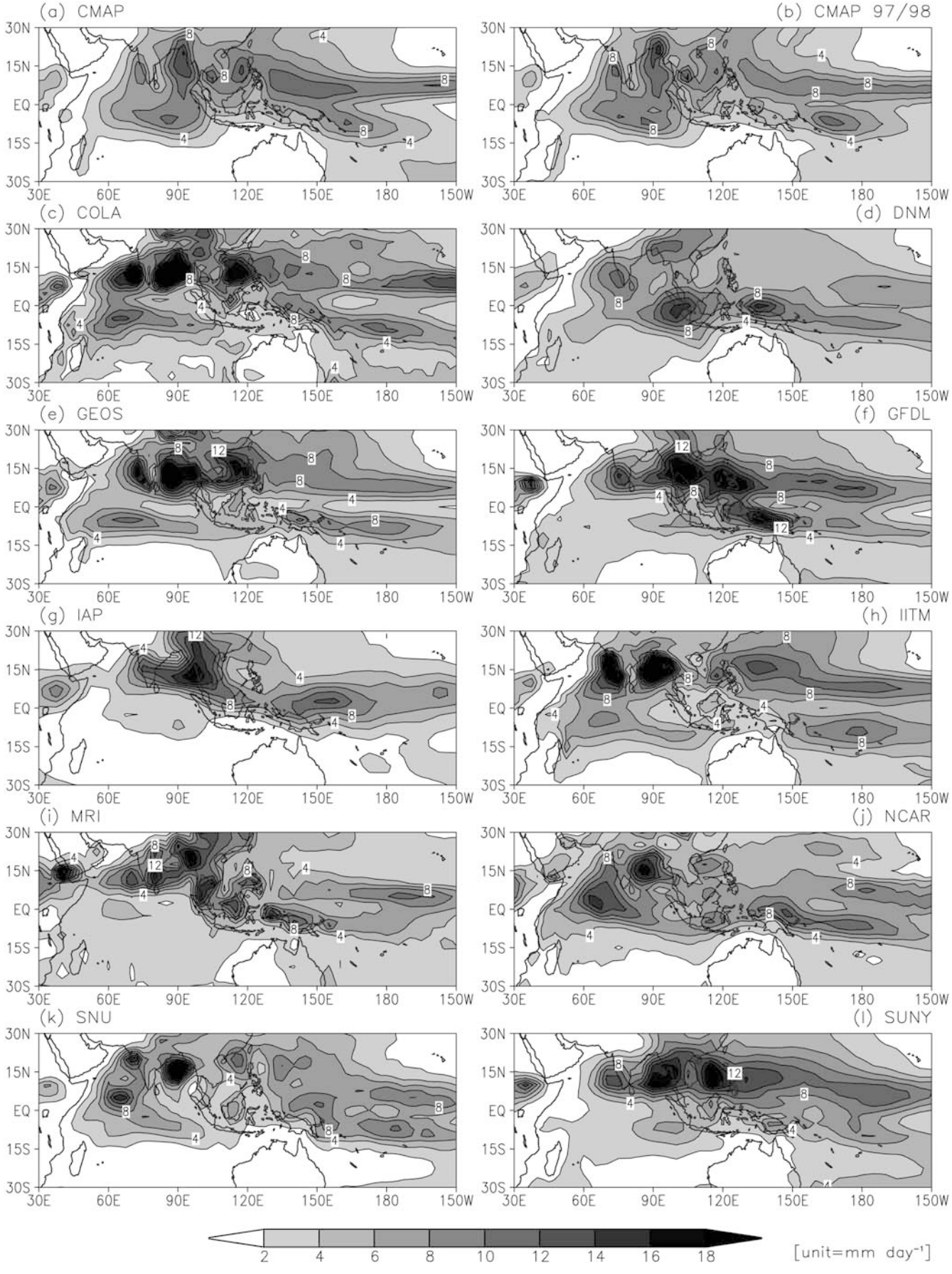
(a) CMAP
(b) CMAP 97/98
(c) COLA
(d) DNM
(e) GEOS
(f) GFDL
(g) IAP
(h) IITM
(i) MRI
(j) NCAR
(k) SNU
(l) SUNY
30N
15N
EQ
15S
30S
30E
60E
90E
120E
150E
180
150W
2
4
6
8
10
12
14
16
18
[unit=mm day⁻¹]

achieving realistic simulations of ISO variability in our weather and climate GCMs.

Acknowledgements This work is a contribution to the Asian–Australian Monsoon GCM Intercomparison Project initiated by the CLIVAR International Monsoon Panel. This project was supported by the Climate Environment System Research Center (CES) which is sponsored by the Korean Science and Engineering Foundation and the Korea Meteorological Administration. Support for the first author was provided by the Atmospheric Sciences Division of the National Science Foundation (NSF; ATM-9712483 and ATM-0094416) and the National Oceanographic and Atmospheric Administration (NOAA; NA16GP2021). Support for V. Krishnamurthy was provided by NSF (ATM-9814295), NOAA (NA96-GP0056), and the National Aeronautics and Space Administration (NAG5-8202).

References

AAMWG, CLIVAR US, Lau WKM, Hastenrath S, Kirtman B, Krishnamurti TN, Lukas R, McCreary J, Shukla J, Shuttleworth J, Waliser D, Webster PJ (2001) An Asian–Australian Monsoon Research Prospectus by the Asian–Australian Monsoon Working Group, pp 46

Annamalai H, Slingo JM (2001) Active/break cycles: diagnosis of the intraseasonal variability of the Asian summer monsoon. Clim Dyn 18: 85–102

Bell GD, Halpert MS, Ropelewski CF, Kousky VE, Douglas AV, Schnell RC, Gelman ME (1999) Climate assessment for 1998. Bull Am Meteorol Soc 80: S1–S48

Betts AK (1986) A new convective adjustment scheme. Part I: Observational and theoretical basis. Quart J Roy Meteor Soc 112: 677–691

Bonan GB (1998) The land surface climatology of the NCAR land surface model (LSM 1.0) coupled to the NCAR Community Climate Model(CCM3). J Climate 11: 1307–1326.

Chou M-D, Ridgway W, Yan M-H (1993) One-parameter scaling and exponential-sum fitting for water vapor and CO2 infrared transmission functions. J Atmos Sci 50: 2294–2303.

Chou M-D, Suarez MJ (1994) An efficient thermal infrared radiation parameterization for use in general circulation models. NASA Tech Memo 104606, Vol. 3, Goddard Space Flight Center, Greenbelt, MD 20771.

Deardorff JW (1978) Efficient prediction of ground surface temperature and moisture, with inclusion of a layer of vegetation. J Geophys Res 83: 1889–1903.

Fennessy MJ, Kinter JL, Kirtman B, Marx L, Nigam S, Schneider E, Shukla J, Straus D, Vernekar A, Xue Y, Zhou J (1994) The simulated Indian Monsoon – a Gcm sensitivity study. J Clim 7: 33–43

Ferranti L, Slingo JM, Palmer TN, Hoskins BJ (1997) Relations between interannual and intraseasonal monsoon variability as diagnosed from AMIP integrations. Q J R Meteorol Soc 123: 1323–1357

Flatau M, Flatau PJ, Phoebus P, Niller PP (1997) The feedback between equatorial convection and local radiative and evaporative processes: the implications for intraseasonal oscillations. J Atmos Sci 54: 2373–2386

Fu X, Wang B, Li T (2002) Impacts of air–sea coupling on the simulation of mean Asian summer monsoon in the ECHAM4 Model. Mon Weather Rev 130: 2889–2904

Gadgil S, Asha G (1992) Intraseasonal variation of the summer monsoon.1. Observational aspects. J Meteorol Soc Jpn 70: 517–527

Gordon CT (1992) Comparison of 30 day integrations with and without cloud-radiation interaction. Mon Wea Rev 120: 1244-1277

Goswami BN (1998) Interannual variations of Indian summer monsoon in a GCM: External conditions versus internal feedbacks. J Clim 11: 501–522

Gregory D, Rowntree PR (1990) A mass flux convection scheme with representation of cloud ensemble characteristics and stability dependent closure. Mon Wea Rev 118: 1483–1506

Gualdi S, Navarra A, Tinarelli G (1999) The interannual variability of the Madden-Julian Oscillation in an ensemble of GCM simulations. Clim Dyn 15: 643–658

Harshvardhan R Davies, Randall DA, Corsetti TG (1987) A fast radiation parameterization for general circulation models. J Geophys Res 92: 1009–1016

Hastenrath S, Greischar L (1993) Changing predictability of Indian monsoon rainfall anomalies. Proc Indian Acad Sci-Earth Planet Sci 102: 35–47

Hayashi Y, Golder DG (1997) United mechanisms for the generation of low- and high-frequency tropical waves.2. Theoretical interpretations. J Meteorol Soc Jpn 75: 775–797

Hendon HH, Salby ML (1994) The life-cycle of the Madden-Julian Oscillation. J Atmos Sci 51: 2225–2237

Hendon HH, Zhang CD, Glick JD (1999) Interannual variation of the Madden-Julian oscillation during austral summer. J Clim 12: 2538–2550

Higgins RW, Shi W (2001) Intercomparison of the principal modes of interannual and intraseasonal variability of the North American monsoon system. J Clim 14: 403–417

Hou Y-T (1990) Cloud-Radiation-Dynamics Interaction. Ph.D. Thesis, University of Maryland at College Park, 209 pp

Ingram WJ, Wood Ward S, Edward J (1996) Radiation. Unified model documentation paper no. 23

Jones C, Schemm JKE (2000) The influence of intraseasonal variations on medium- to extended-range weather forecasts over South America. Mon Weather Rev 128: 486–494

Kalnay E, Kanamitsu M, Kistler R, Collins W, Deaven D, Gandin L, Iredell M, Saha S, White G, Woollen J, Zhu Y, Chelliah M, Ebisuzaki W, Higgins W, Janowiak J, Mo KC, Ropelewski C, Wang J, Leetmaa A, Reynolds R, Jenne R, Joseph D (1996) The NCEP/NCAR 40-year reanalysis project. Bull Am Meteorol Soc 77: 437–471

Kang I, An S, Joung C, Yoon S, Lee S (1989) 30–60 day oscillation appearing in climatological variation of outgoing longwave radiation around East Asia during summer. J Korean Meteorol Soc 25: 149–160

Kang IS, Ho CH, Lim YK, Lau KM (1999) Principal modes of climatological seasonal and intraseasonal variations of the Asian summer monsoon. Mon Weather Rev 127: 322–340

Kang IS, Lau KM, Shukla J, Krishnamurthy V, Schubert SD, Waliser DE, Stern WF, Satyan V, Kitoh A, Meehl GA, Kanamitsu M, Galin VY, Kim JK, Sumi A, Wu G, Liu Y (2002a) Intercomparion of GCM simulated anomalies associated with the 1997–98 El Niño. J Clim 15: 2791–2805

Kang IS, K. J, Wang B, Lau KM, Shukla J, Schubert SD, Waliser DE, Krishnamurthy V, Stern WF, Satyan V, Kitoh A, Meehl GA, Kanamitsu M, Galin VY, Kim JK, Sumi A, Wu G, Liu Y (2002b) Intercomparison of the climatological variations of Asian summer monsoon precipitation simulated by 10 GCMs. Clim Dyn 19: 383–395

Katayama A (1978) Parameterization of the planetary boundary layer in atmospheric general circulation models. Kisyo Kenkyu Note No. 134, Meteorological Society of Japan, 153–200 (in Japanese)

Kemball-Cook S, Wang B (2001) Equatorial waves and air–sea interaction in the Boreal summer intraseasonal oscillation. J Clim 14: 2923–2942

Kemball-Cook S, Wang B, Fu X (2002) Simulation of the ISO in the ECHAM4 model: the impact of coupling with an ocean model. J Atmos Sci 59: 1433–1453

Kiehl JT (1994) On the Observed near cancellation between longwave and shortwave cloud forcing in tropical regions. Journal of Climate Vol. 7, No. 4, pp. 559–565

Kiehl JT, Hack JJ, Bonan G, Boville B, Williamson D, Rasch P (1998) The National Center for Atmospheric Research Community Climate Model (CCM3). J Climate 11: 1131–1149
Kitoh A, Yamazaki K, Tokioka T (1988) Influence of soil moisture and surface albedo changes over the African tropical rain forest on summer climate investigated with the MRI GCM-I. J Meteor Soc Japan 66: 65–86
Krishnamurthy V, Shukla J (2000) Intraseasonal and interannual variability of rainfall over India. J Clim 13: 4366–4377
Krishnamurti TN, Subramaniam M, Daughenbaugh G, Oosterhof D, Xue JH (1992) One-month forecasts of wet and dry spells of the monsoon. Mon Weather Rev 120: 1191–1223
Kumar KK, Rajagopalan B, Cane MA (1999) On the weakening relationship between the Indian monsoon and ENSO. Science 284: 2156–2159
Lacis AA, Hansen JE (1974) A parameterization for the absorption of solar radiation in the Earth's atmosphere. J Atmos Sci 31: 118–133
Lal M, Cubasch U, Perlwitz J, Waszkewitz J (1997) Simulation of the Indian monsoon climatology in ECHAM3 climate model: sensitivity to horizontal resolution. Int J Climatol 17: 847–858
Lau KM, Chan PH (1986) Aspects of the 40–50 day oscillation during the northern summer as inferred from outgoing longwave radiation. Mon Weather Rev 114: 1354–1367
Lau KM, Chan PH (1988) Intraseasonal and interannual variations of tropical convection – a possible link between the 40–50 day oscillation and Enso. J Atmos Sci 45: 506–521
Lau KM, Yang GJ, Shen SH (1988) Seasonal and intraseasonal climatology of summer monsoon rainfall over East-Asia. Mon Weather Rev 116: 18–37
Lawrence DM, Webster PJ (2001) Interannual variations of the intraseasonal oscillation in the south Asian summer monsoon region. J Clim 14: 2910–2922
Le Treut H, Li Z-X (1991) Sensitivity of an atmospheric general circulation model to prescribed SST changes: feedback effects associated with the simulation of cloud optical properties. Clim Dynam 5: 175–187
Liang XZ, Samel AN, Wang WC (1995) Observed and Gcm simulated decadal variability of monsoon rainfall in East China. Clim Dyn 11: 103–114
Liu YM, Chan JCL, Mao JY, Wu GX (2002) The role of Bay of Bengal convection in the onset of the 1998 South China Sea summer monsoon. Mon Weather Rev (in press)
Lo F, Hendon HH (2000) Empirical extended-range prediction of the Madden-Julian oscillation. Mon Weather Rev 128: 2528–2543
Lucas LE, Waliser DE, Xie P, Janowiak JE, Liebmann B (2001) Estimating the satellite equatorial crossing time biases in the daily, global outgoing longwave radiation dataset. J Clim 14: 2583–2605
Madden RA, Julian PR (1994) Observations of the 40–50-day tropical oscillation – a review. Mon Weather Rev 122: 814–837
Maloney ED, Hartmann DL (2000) Modulation of eastern North Pacific hurricanes by the Madden-Julian oscillation. J Clim 13: 1451–1460
Manabe S, Smagorinsky J, Strickler RF (1965) Simulated climatology of a general circulation model with a hydrologic cycle. Mon Wea Rev 93: 769–798
Martin GM (1999) The simulation of the Asian summer monsoon, and its sensitivity to horizontal resolution, in the UK Meteorological Office Unified Model. Q J R Meteorol Soc 125: 1499–1525
McPhaden MJ (1999) Climate oscillations – genesis and evolution of the 1997–98 El Nino. Science 283: 950–954
Mo KC (2000a) The association between intraseasonal oscillations and tropical storms in the Atlantic basin. Mon Weather Rev 128: 4097–4107
Mo KC (2000b) Intraseasonal modulation of summer precipitation over North America. Mon Weather Rev 128: 1490–1505
Mo KC (2001) Adaptive filtering and prediction of intraseasonal oscillations. Mon Weather Rev 129: 802–817
Mo KC, Higgins RW (1998) The Pacific–South American modes and tropical convection during the Southern Hemisphere winter. Mon Weather Rev 126: 1581–1596
Moorthi S, Suarez MJ (1992) Relaxed Arakawa-Schubert: A parameterization of moist convection for general circulation models. Mon Wea Rev 120: 978–1002
Murakami T, Chen LX, Xie A, Shrestha ML (1986) Eastward propagation of 30–60 day perturbations as revealed from outgoing longwave radiation data. J Atmos Sci 43: 961–971
Nakajima T, Tanaka M (1986) Matrix formulation for the transfer of solar radiation in a plane-parallel scattering atmosphere. J Quant Spectrosc Radiat Transfer 35: 13–21
Nakazawa T (1992) Seasonal phase lock of intraseasonal variation during the Asian summer monsoon. J Meteorol Soc Jpn 70: 257–273
NoguesPaegle J, Mo KC (1997) Alternating wet and dry conditions over South America during summer. Mon Weather Rev 125: 279–291
Paegle JN, Byerle LA, Mo KC (2000) Intraseasonal modulation of South American summer precipitation. Mon Weather Rev 128: 837–850
Parthasarathy B, Kumar KR, Deshpande VR (1991) Indian-summer monsoon rainfall and 200-Mbar meridional wind index – application for long-range prediction. Int J Climatol 11: 165–176
Preisendorfer RW, Zwiers EW, Barnett TP (1981) Foundations of principal component selection rules. Scripps Institution of Oceanography, Rep 81-7, La Jolla, CA, pp 200
Ramesh KJ, Iyengar GR (1999) Characteristics of medium range rainfall forecasts of the Asian summer monsoon. Int J Climatol 19: 627–637
Reynolds RW, Smith TM (1994) Improved global sea-surface temperature analyses using optimum interpolation. J Clim 7: 929–948
Richman MB (1986) Rotation of principal components. J Clim 6: 293–335
Richman MB, Easterling WE (1988) Procrustes target analysis – a multivariate tool for identification of climate fluctuations. J Geophys Res-Atmos 93: 10,989–11,003
Schemm J –K, Schubert S, Terry J, Bloom S, Sud Y (1992) Estimates of monthly mean soil moisture for 1979-89, NASA Tech. Memo. No. 104571, Goddard Space Flight Center, Greenbelt, MD 20771
Schwarzkopf MD, Fels SB (1991) The simplified exchange method revisited: An accurate, rapid method for computation of infrared cooling rates and fluxes. J Geophys Res 96: 9075–9096
Shi GY (1981) An accurate calculation and the infrared transmission function of the atmospheric constituents. Ph.D. Thesis, Dept. of Sci., Tohoku University of Japan. pp. 191
Shibata K, Aoki T (1989) An infrared radiative scheme for the numerical models of weather and climate. J Geophys Res 94: 14923–14943
Slingo A, Wilderspin RC (1986) Development of a revised longwave radiation scheme for an atmospheric general circulation model. Quart J Roy Meteor Soc 112: 371–386
Slingo A (1989) A GCM parameterization for the shortwave radiative properties of water clouds. J Atmos Sci 46: 1419–1427
Slingo JM, Ritter B (1985) Cloud prediction in the ECMWF model. ECMWF Tech. Report No. 46, European Center for Medium-Range Weather Forecasts, Reading, England, 48pp
Slingo JM (1987) The development and verification of a cloud prediction model for the ECMWF model. Quart. J Roy Meteor Soc 13: 899–927
Slingo JM, Sperber KR, Boyle JS, Ceron JP, Dix M, Dugas B, Ebisuzaki W, Fyfe J, Gregory D, Gueremy JF, Hack J, Harzallah A, Inness P, Kitoh A, Lau WKM, McAvaney B, Madden R, Matthews A, Palmer TN, Park CK, Randall D, Renno N (1996) Intraseasonal oscillations in 15 atmospheric general circulation models: results from an AMIP diagnostic subproject. Clim Dyn 12: 325–357

Slingo JM, Rowell DP, Sperber KR, Nortley E (1999) On the predictability of the interannual behaviour of the Madden-Julian Oscillation and its relationship with El Nino. Q J R Meteorol Soc 125: 583–609

Smith RNB (1990a) Subsurface, surface and boundary layer processes, Unified Model Doc. Paper 24, Available at Nat. Met. Lib., Bracknell

Smith RNB (1990b) A scheme for predicting layer clouds and their water content in a General Circulation Model. Quart J Roy Meteor Soc 116: 435–460

Soman MK, Slingo J (1997) Sensitivity of the Asian summer monsoon to aspects of sea-surface-temperature anomalies in the tropical Pacific Ocean. Q J R Meteorol Soc 123: 309–336

Sperber KR, Palmer TN (1996) Interannual tropical rainfall variability in general circulation model simulations associated with the atmospheric model intercomparison project. J Clim 9: 2727–2750

Sperber KR, Slingo JM, Inness PM, Lau WKM (1997) On the maintenance and initiation of the intraseasonal oscillation in the NCEP/NCAR reanalysis and in the GLA and UKMO AMIP simulations. Clim Dyn 13: 769–795

Sperber KR, Slingo JM, Annamalai H (2000) Predictability and the relationship between subseasonal and interannual variability during the Asian summer monsoon. Q J R Meteorol Soc 126: 2545–2574

Sperber KR, Brankovic C, Deque M, Frederiksen CS, Graham R, Kitoh A, Kobayashi C, Palmer T, Puri K, Tennant W, Volodin E (2001) Dynamical seasonal predictability of the Asian summer monsoon. Mon Weather Rev 129: 2226–2248

Sud YC, Walker GK (1992) A review of recent research on improvement of physical parameterizations in the GLA GCM. In Physical Processes in Atmospheric Models, D.R. Sikka and S.S. Singh (eds.), Wiley Eastern Ltd., New Delhi, 422–479

Tokioka T, Yamazaki K, Yagai I, Kitoh A (1984) A description of the Meteorological Research Institute atmospheric general circulation model (MRI GCM-I). MRI Tech. Report No. 13, Meteorological Research Institute, Ibaraki-ken, Japan, 249 pp

Tokioka T, Yamazaki K, Kitoh A, Ose T (1988) The equatorial 30-60 day oscillation and the Arakawa-Schubert penetrative cumulus parameterization. J Meteor Soc Japan 66: 883–901

Volodin EM, Lykossov VN (1998) Parameterization of heat and moisture transfer in the soil-vegetation system for use in atmospheric general circulation models: 1. Formulation and simulations based on local observational data. Izvestiya Atmospheric and Oceanic Physics 34: 405–416 (Translated from Izvestiya AN. Fizika Atmosfery i Okeana)

Waliser DE, Graham NE, Gautier C (1993) Comparison of the highly reflective cloud and outgoing longwave radiation datasets for use in estimating tropical deep convection. J Clim 6: 331–353

Waliser DE, Lau KM, Kim JH (1999a) The influence of coupled sea surface temperatures on the Madden-Julian oscillation: a model perturbation experiment. J Atmos Sci 56: 333–358

Waliser DE, Jones C, Schemm JKE, Graham NE (1999b) A statistical extended-range tropical forecast model based on the slow evolution of the Madden-Julian oscillation. J Clim 12: 1918–1939

Waliser D, Zhang Z, Lau KM, Kim JH (2001) Interannual sea surface temperature variability and the predictability of tropical intraseasonal variability. J Atmos Sci 58: 2595–2614

Waliser DE, Lau KM, Stern W, Jones C (2003a) Potential predictability of the Madden-Julian Oscillation. Bull Am Meteorol Soc 84: 33–50

Waliser DE, Stern W, Schubert S, Lau KM (2003b) Dynamic Predicts of Intraseasonal Variability Associated with the Asien Summer Monsoon. Quart Royal Meteor Soc: in press

Wang B, Rui H (1990) Synoptic climatology of transient tropical intraseasonal convection anomalies – 1975–1985. Meteorol Atmos Phys 44: 43–61

Wang B, Xu XH (1997) Northern Hemisphere summer monsoon singularities and climatological intraseasonal oscillation. J Clim 10: 1071–1085

Wang B, Xie XS (1997) A model for the boreal summer intraseasonal oscillation. J Atmos Sci 54: 72–86

Wang B, Kang I.-S., Lee J.-Y. (2003) Asian-Australien Monsoon Variability During 1997–1998 El Nino Simulated by Eleven AGCMs. Clim Dyn: in press

Webster PJ, Magana VO, Palmer TN, Shukla J, Tomas RA, Yanai M, Yasunari T (1998) Monsoons: processes, predictability, and the prospects for prediction. J Geophys Res-Oceans 103: 14,451–14,510

Wheeler M, Weickmann KM (2001) Real-time monitoring and prediction of modes of coherent synoptic to intraseasonal tropical variability. Mon Weather Rev 129: 2677–2694

Wu GX, Zhang YS (1998) Tibetan Plateau forcing and the timing of the monsoon onset over South Asia and the South China Sea. Mon Weather Rev 126: 913–927

Wu MLC, Schubert S, Kang IS, Waliser DE (2002) Forced and free intra-seasonal variability over the South Asian Monsoon region simulated by 10 AGCMs. J Clim 15: 2862–2880

Xie PP, Arkin PA (1997) Global precipitation: a 17-year monthly analysis based on gauge observations, satellite estimates, and numerical model outputs. Bull Am Meteorol Soc 78: 2539–2558

Xue Y-K, Sellers PJ, Kinter II JL, Shukla J (1991) A simplified biosphere model for global climate studies. J Climate 4: 345–364

Yasunari T (1979) Cloudiness fluctuations associated with the Northern Hemisphere summer monsoon. J Meteorol Soc Jpn 57: 227–242

Yasunari T (1980) A quasi-stationary appearance of the 30–40 day period in the cloudiness fluctuations during the summer monsoon over India. J Metorol Soc Jpn 59: 336–354

Zachary A, Randall D (1999) Sensitivity of the simulated Asian summer monsoon to parameterized physical processes. J Geophys Res 104: 12,177–12,191

Zhang GJ, McFarlane NA (1995) Sensitivity of climate simulations to the parameterization of cumulus convection in the Canadian Climate Centre general circulation model. Atmos-Ocean 33: 407–446